1-1-2006

Satellite-based remote sensing of suspended sediments along the coast of Guyana.

Sajid Rashid Ahmad
University of Windsor

SATELLITE-BASED REMOTE SENSING OF SUSPENDED SEDIMENTS ALONG THE COAST OF GUYANA

By

SAJID RASHID AHMAD

A Thesis Submitted
to the Faculty of Graduate Studies and Research
through Earth Sciences
In Partial Fulfillment of the Requirements for
the Degree of Master of Science at the
University of Windsor

Windsor, Ontario, Canada

2006

Your file Votre référence
ISBN: 978-0-494-35911-2
Our file Notre référence
ISBN: 978-0-494-35911-2

ABSTRACT

This study utilized Landsat Multi-spectral, Thematic Mapper, and Enhanced Thematic Mapper + data from the Guyana coast for obtaining insights on the temporal variations and spatial distribution of suspended sediments in the nearshore environment.

Data from twenty-five spectral bands representing 1985, 1992, 1999 and 2002 were analyzed with the Idrisi and the ArcGIS 9.0 software. Results from the principle components analysis (PCA) highlighted the importance of Band 2 (0.6 - 0.7 micrometers) for the 1985 image, Band 3 (0.63 - 0.69 micrometers) for the 1992 image, Band 2 (0.52 - 0.60 micrometers) for the 1999 image and Band 3 (0.63 - 0.69) for the 2002 image. The PCA bands were integrated in ArcGIS 9.0, and sediment polygons were delineated. Sediment difference maps were produced which demonstrated that suspended sediments in the coastal waters increased for the period 1985 to 2002.

The obtained results permitted testing and acceptance of two hypotheses. The spectral wavelength range of 0.52 - 0.7 micrometers was found to be very appropriate for identifying suspended sediments in coastal waters. The regression plot and percentage difference maps permitted the claim that there were temporal increases in suspended sediments in the coastal waters of Guyana.

ACKNOWLEDGMENTS

My thesis would not have been completed without the encouragement, supervision and professional guidance of my faculty advisor, Dr. V.C. Lakhan. He provided me with maximum support both in the field and at the University. My sincere thanks to Dr. Lakhan for his outstanding assistance. I also provide sincere acknowledgments to Dr. Maria Cioppa and Dr. Rajesh Seth for their academic guidance and support.

The many personnel in Guyana are also acknowledged for their friendship and field assistance. The data provided by personnel from the Ministries in Guyana are greatly appreciated.

My sincere thanks also to my wife, Mona, children (Aamna, Mujtaba and Momna) and family members, especially my mother. Their help has been invaluable.

Special thanks are also extended to all my friends and colleagues at the University of Windsor, and the University of the Punjab, Lahore, Pakistan.

TABLE OF CONTENTS

LIST OF TABLES

LIST OF FIGURES

CHAPTER 1

1.0 INTRODUCTION AND STUDY AREA

1.1 Introduction

Data from satellite-based remote sensing systems are now providing valuable new perspectives on the broad scale, dynamic characteristics of coastal water bodies. Ever since the launch of the Earth Resources LANDSAT 1 satellite on July 23, 1972 early researchers (for example, Klemas et al., 1973; Ritchie et al., 1976; Welby, 1978 and Bhargava and Mariam, 1990) and more recent investigators (for example, Mikkelsen, 2002; Doxaran et al., 2003; Li et al., 2003, Doxaran et al., 2004) have shown that remote sensors are very useful to study the turbidity in water bodies. Turbidity refers to the amount of light transmitted through water, and remote sensing investigations focus on the influence of suspended sediments on turbidity. The success of satellite-based remote sensing of suspended sediments could be attributed to the fact that remote sensing provides a far more synoptic view of the turbid patterns in a water body. Finding the suspended sediment concentration in coastal waters with remote sensing techniques has a major advantage over *in situ* measurements which are taken from a limited number of sampling points, and are not normally representative of the entire water body. Discrete point source measurements are only representative of sediments existing in the rather confined sample area. With multi-spectral remote sensing, it is possible to determine the relationship between the digital reflectance values measured by the remote sensor, and the suspended sediments over the entire study area. In brief, remote sensors are used to measure the changes in the spectral signature reflected from the water surface. The

measured changes can then be related by empirical or analytical models of suspended sediments.

Since remote sensing has proven to be an efficient tool for mapping suspended sediments and turbidity in coastal waters, researchers from around the globe have used data from various satellite-based remote sensing systems (for example, LANDSAT, SPOT, MODIS, RADARSAT) to investigate various aspects of turbidity in coastal waters, including suspended particulate matter and water quality. Knowing the suspended sediment concentration points out areas of heavy pollution and erosion in the water body making it a valuable tool for water quality assessment. Suspended sediment concentration is also a good indicator of general circulation patterns in coastal waters. In addition, waters with high concentrations of suspended sediments have impacts on aquatic ecosystems and the utilization of water bodies for recreational purposes.

While satellite-based investigations on suspended sediment concentrations in the coastal environment have been conducted by researchers (for example, Khorram and Cheshire, 1985; Puls et al., 1994; Estournel et al., 1997; Mancebo et al., 1997; Islam et al., 2001; Kiyomoto et al., 2001) from several countries, there is, nevertheless, a paucity of remote sensing research on suspended sediment concentrations along the coast of Guyana. Observations from field researchers (for example, Allersma, 1971; and Eisma and van der Marel, 1971) found that the Guyana coast is under the constant influence of massive loads of suspended sediments. To obtain insights on the temporal variations in suspended sediments along the coast of Guyana this research will, therefore, analyze satellite-based remotely sensed data. Remote sensing data obtained from the MSS (Multi-

Spectral Scanner), TM (Thematic Mapper) and ETM+ (Enhanced Thematic Mapper) sensors will be analyzed to investigate whether suspended sediments have decreased or increased over time along the coast of Guyana.

1.2 Significance and Objectives of Research

As far as can be ascertained, this is the first study to assess the temporal variations in suspended sediments with the use of data from three different types of sensors (MSS, TM and ETM+). This is very significant because it will establish the usefulness of specific sensors for assessing variations in suspended sediment concentrations in coastal waters. A primary objective will be to identify appropriate spectral bands which are associated with suspended sediments in coastal waters. The results from this study will serve to fulfill one of the objectives of this research which is to determine whether suspended sediments are increasing or decreasing over time along the Guyana coast. Should sediments be increasing, then important conclusions could be drawn on the impacts of deforestation in the Amazon Basin on increases in suspended particulate matter in the coastal waters off the northern coast of South America. By combining remote sensing and GIS techniques, this study will have the other objective of providing resource planners and coastal managers with a cost effective method for evaluating and visualizing water quality characteristics in the coastal zone at different temporal and spatial scales.

1.3 Hypotheses

To fulfill the objectives of this research the following hypotheses will be tested:

a) There is a strong association between suspended sediments in coastal waters and specific spectral bands of remote sensing sensors.

b) There is a distinct temporal increase in suspended sediments in the nearshore areas of the coastal environment of Guyana.

1.4 The Study Area

The study area is located on a portion of the northeast coast of the South American continent known as the Guiana coast and stretches some 1600 km between the mouths of the Orinoco and Amazon Rivers. It forms the coastline of French Guiana, Surinam, Guyana, and parts of the Brazilian and Venezuelan coasts. Emphasis is on the Guyana coast which has a length of about 435 km (see Figure 1.1). The Guyana coast extends from Punta Playa near the Venezuelan border in the west to the Corentyne River in the east. The coast is associated with a generally flat coastal plain which is approximately 2.5 to 4.0 m below high tide level (Lakhan, 1991). Although the coastal zone is the smallest physiographic area and occupies less than 5% of Guyana's surface area, yet more than 90% of the country's population live in the coastal environment (Lakhan, 1994). The residents of the heavily settled coastal environment are faced with numerous environmental issues principally among them recurring episodes of flooding and erosional problems.

Erosion along the coast is a consequence of combined sedimentological and hydrodynamic processes. Some of these processes have been described in previous studies (for example, Allersma, 1971; Augustinus, 1987; and Lakhan and Pepper, 1997). Other than the influence of waves and tides, the coast is affected by the continuous presence of massive loads of sediments. The entire offshore coast of Guyana receives an immense amount of fine sediments with estimates of 1-2 x 10^8 tonnes per year, which is

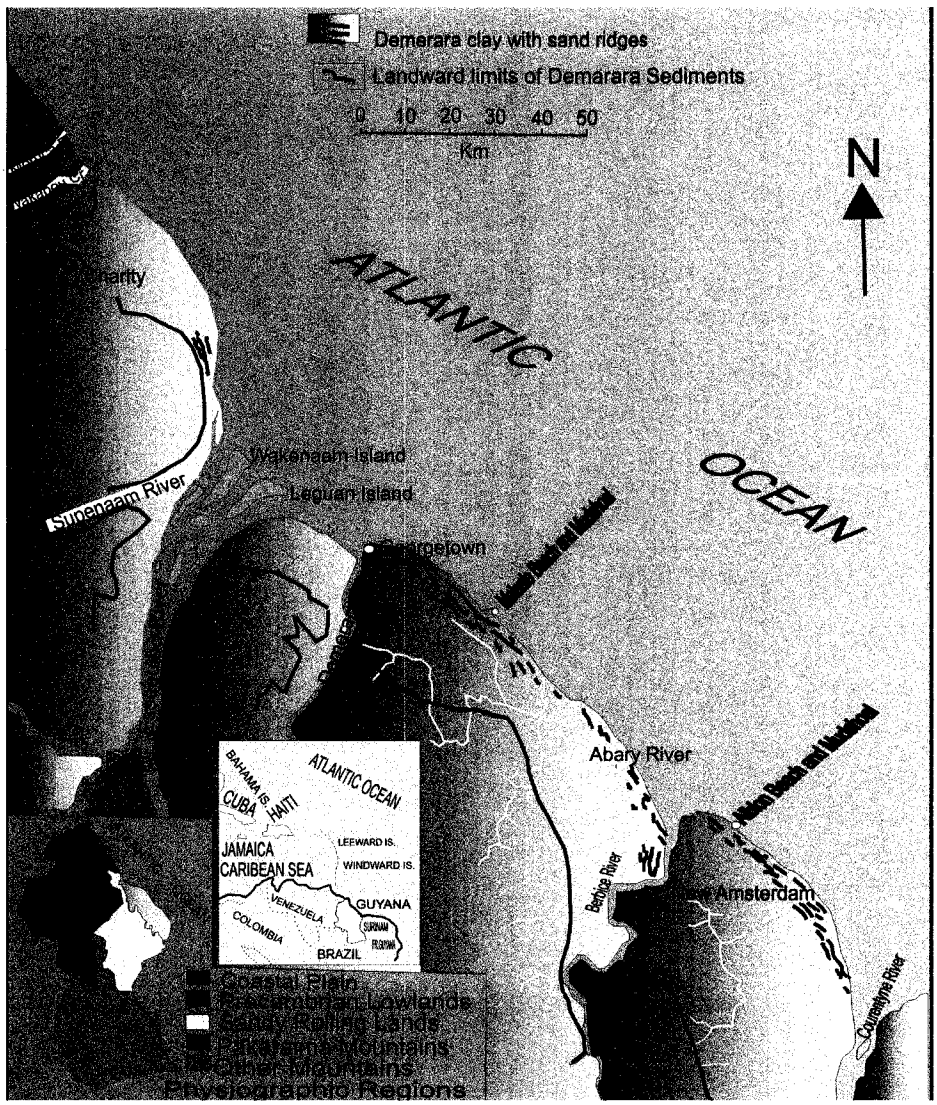

Figure 1.1: Regional Setting of the Guyana Coast.
Source: Lakhan et al. (2002)

about 20-40% of the total yearly sediment load of the Amazon. With the exception of the Essequibo River, most of the major rivers in Guyana have been found to contribute a relatively low percentage of suspended sedimentary material in the coastal zone (Eisma and van der Marel, 1971). Analyses of sediment samples found that organic matter constituted 1-2% of the sediment, with the bulk consisting of the clay minerals kaolinite and illite, with 10-20% montmorillonite, and about 20% quartz (Allersma, 1971).

A broad plume of suspended sediments is transported from the mouth of the Amazon River in a northwesterly direction by the Equatorial Current, and subsequently by the Guiana Current (Figure 1.2). In addition to the annual transport of an immense amount of suspended sediments there is also the transport of sediments in the form of

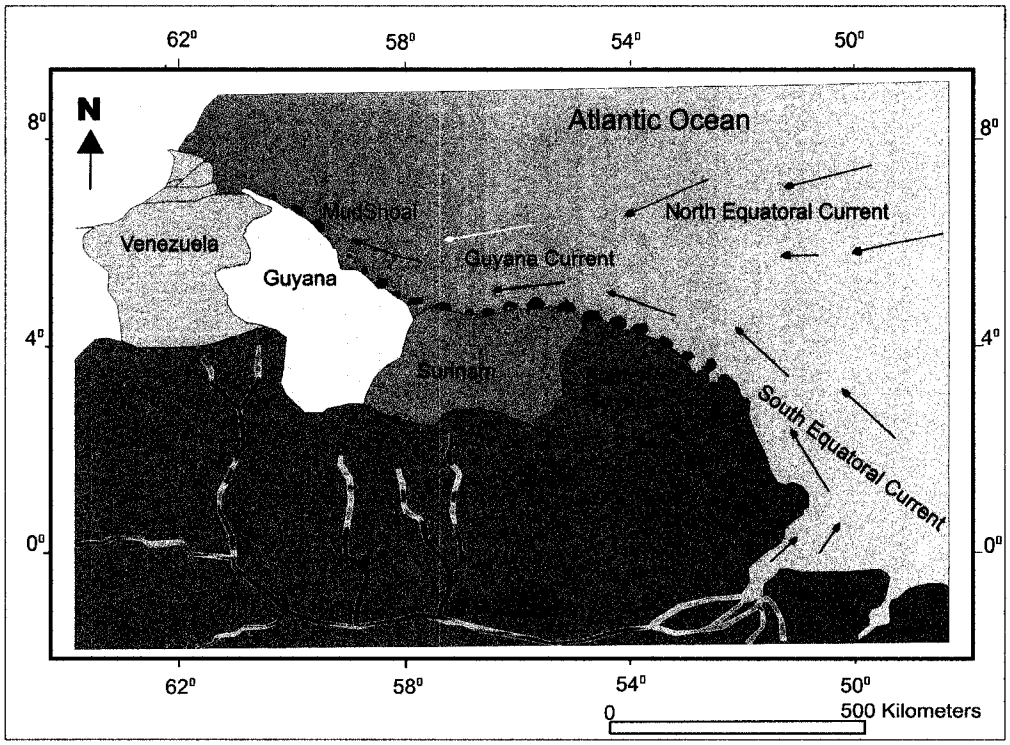

Figure 1.2: Currents Along the Guyana Coast.
Source: Delft Hydraulics Laboratory, 1962

mudbanks. The mudbanks move westward at a rate of 1.5 km per year from the Amazon and reach the Essequibo River in Guyana after about 1000 years (Eisma and van der Marel, 1971). The movement of mudbanks is accompanied by a pattern of erosion and accretion of the adjacent coast (Allersma, 1971; Augustinus, 1987). Accretion takes place on the coast directly opposite the mudbanks, while erosion occurs along the coast opposite the troughs situated between two mudbanks. The study by Lakhan et al. (2002) demonstrated that there are distinct variations in sediment sizes in eroding and accreting areas along the coast (Figure 1.3). The accreting areas are dominated by fine grained sediments.

The movement and deposition of suspended sediments affect not only coastal morphology and hydrodynamics, but also have impacts on harbors, navigation channels, fisheries, aquatic ecology and water quality (Lakhan and Ahmad, 2005). Although the entire length of the coastline is influenced by the presence of suspended sediments, this thesis will focus on suspended sediments occurring along the most populated and economically viable section of the Guyana coast.

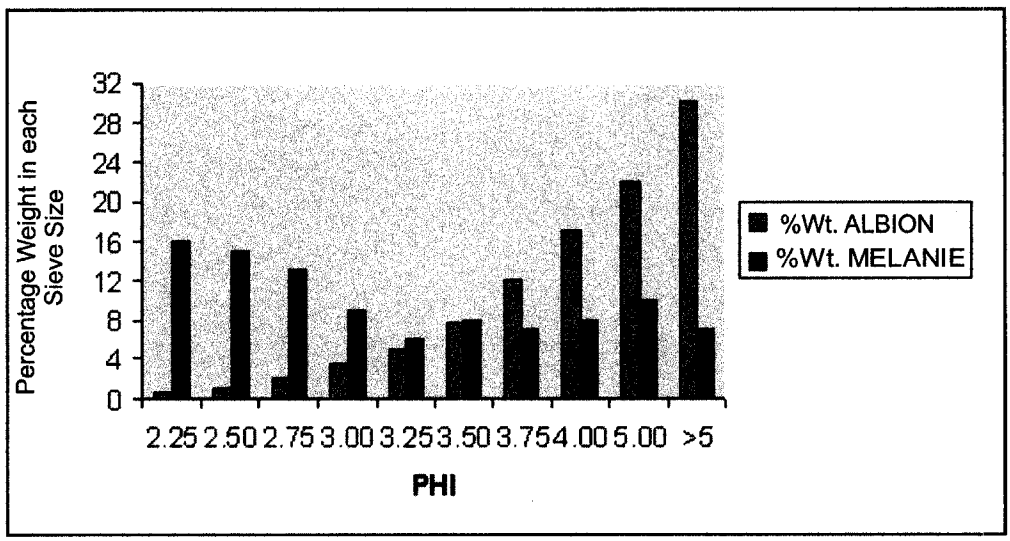

Figure 1.3: Variations in Sediments Along the Coast of Guyana (locations of place names, Albion and Melanie, are on Figure 1.1).
Source: Lakhan et al. (2002)

CHAPTER 2

2.0 LITERATURE REVIEW

2.1 General Remarks on the Use of Remote Sensing for Investigating Suspended Sediments

Satellite-based remote sensing systems are now widely used to monitor large areas of water bodies on a repetitive basis. Since remote sensing can provide up-to-date information on water bodies and associated characteristics resource managers are provided with a cost effective means of acquiring timely data on not only turbidity but also water quality. Essentially, substances in surface waters are known to change the radiation and reflectivity characteristics of the surface water. Remote sensing sensors can, therefore, be used to measure the changes in the spectral signature back-scattered from the water surface. The measured changes can then be related by empirical or analytical models of suspended sediments. The development of models to demonstrate the relationships between suspended sediment concentrations and reflectance took the form of four stages of research (Curran et al., 1987). The first step taken by researchers was to derive the relationship between reflectance and suspended sediment concentration. The second step was to derive a model of the relationship. The third step was to use the model by inverting it, to estimate suspended sediment concentration over large areas. The fourth step was to assess the accuracy of the suspended sediment concentration predictions and to assess the errors.

One of the first linear models was that of Ritchie et al. (1974) which took the form of

$$Y = AX + B \qquad (1)$$

where Y is the remote sensing measurement (i.e., reflectance) and X is the water quality parameter (i.e., suspended sediments). A and B are empirically derived coefficients.

With the use of SPOT HRV and LANDSAT TM data, Forget and Ouillon (1998) established a relationship between satellite reflectance and total suspended matter. They applied linear polynomial, loglinear and log-log relationships, and found that the loglinear relationship gave the best correlation. This took the form of

$$R_k = a_k \log_{10} TSM + b_k \quad (2)$$

where R_k is the relationship, and a_k and b_k are empirical factors. TSM is the total suspended matter.

This literature review will provide evidence of the aforementioned relationships. Other studies have been done to establish the claim that there are distinct relationships between water surface reflectance and suspended sediment concentrations.

2.2 Overview of Satellite Investigations

The early study by Ritchie et al. (1976) attempted to find the optimum wavelength for quantitatively determining suspended sediment concentration of surface water from remote platforms. They studied six reservoirs in northern Mississippi, United States. The reflected and incident solar radiation were measured from a boat with a pointable spectroradiometer at each site. The suspended sediment concentration was also found at each site at the secchi extinction depth. They felt that a linear regression equation best fit the relationship between the concentration of total solids in the water and solar radiation and reflectance (ratio of reflected solar radiation to incident solar radiation). The study found that the amount of solar radiation reflected from the water

surface varied with the amount of suspended sediment and the wavelength it was recorded at. They felt the best region of the spectrum for prediction of suspended sediment concentration was 700 to 800 nanometers.

Various other studies have been conducted combining *in situ* measurements and satellite data from various sensors in order to relate and model spectral properties and suspended sediments. To emphasize the research done with the use of different types of sensors the literature will review the findings from specific sensors, especially the MSS, TM and ETM+ systems. Before this is done an overview will, however, be provided on the other types of sensors used to determine suspended sediment concentrations.

Olariu et al. (2002) used ASTER (Advanced Spaceborne Thermal Emission and Reflection Radiometer) data to calculate suspended sediment concentrations in the Red River delta. Transformation of digital numbers yielded estimates of suspended sediment concentrations between 0 and 800 mg/l, but the method had some limitations for concentrations higher than 600 mg/l. The remote sensing datasets which were used showed that during the high discharge period sediments were visible as far as 8 km away from the delta front.

Baghadadi et al. (2004) conducted a comparative study between European Remote Sensing Satellite (ERS) and RADARSAT, and ASTER images and found that the low angle radar was more suitable for detecting mudbanks, whereas high angle radar is more appropriate for monitoring coastline changes.

The Moderate Resolution Imaging Spectra Radiometer (MODIS) satellite sensors are used to provide observations of the ocean's surface suspended particle matter (SPM) concentrations. Results provide valuable information on sediments in coastal

environments, particularly on the origin and fate of suspended sediments over great distances (Friodefond et al., 2004).

MODIS data were used by other researchers (for example, Li et al., 2003; and Mobasheri and Hamid, 2004) to study suspended sediments. They stated that MODIS channel 4, with 550 nm wavelength, was a good correlation with the total density in high visibility situations. Mobasheri (2005) used the MODIS sensor to examine suspended sediment concentrations in the Bahmansheer estuary at the northeast of the Persian Gulf. A strong positive relationship was found to exist between suspended sediment concentrations and spectral radiance. The reflection was concentrated mainly in the first seven MODIS bands.

Several researchers (for example, Doxaran et al., 2002b; Friodefond et al., 2004; and Fromard et al., 2004) focused on SPOT data. They found that remote sensing reflectance increased with SPM concentrations. Doxaran et al. (2002b) obtained the best correlation between the near infrared band (790-890 nm) and reflectance ratios. Friodefond et al. (2004), however, stated that wavelength 610-680 nm was better for determining SPM concentration in the shallow water zone.

Some other researchers (for example, Ruddick et al., 1998, and Walker et al., 2002) used data from AVHRR (Advanced Very High Resolution Radiometer) and found the 580-680 nm wavelength was best for estimating SPM concentration. Kiyomoto et al. (2001) used the Coastal Zone Colour Scanner (CZCS) data and stated that 670 nm wavelength was good to determine SPM concentrations.

González (2005) evaluated the dynamics of three river plumes in the Mayaguez Bay and determined distinct characteristics between them with data from the Airborne

Visible/Infrared Image Spectrometer (AVRIIS). The applied algorithm for detecting suspended sediment concentrations demonstrated that remote sensing is a useful tool for detecting changes in ocean color produced by suspended sediments.

The concentration of suspended sediments in coastal waters was also examined by Xiaoqin et al. (2005). They found that the 1.1 km resolution of AVHRR and SeaWiFS (Sea-viewing Wide Field of view Sensor) data was too coarse for calculating suspended sediments. However, TM and ASTER data were found to be somewhat applicable for developing algorithms for the calculation of suspended sediment in coastal waters.

2.3 Multi Spectral Scanner (MSS) Studies

Though designed primarily as a Land Oriented Sensing System, the LANDSAT Multi-Spectral Scanner (MSS) is widely used in limnologic and oceanographic studies. Several researchers (for example, Johnson and Harris, 1980; Jacobberger et al., 1983; Khorram and Cheshire, 1985; Ritchie and Cooper, 1988; Mackinnon et al., 1996; Zhu, 2001, and Siddiqui and Maajid, 2004) have used MSS data for water quality monitoring and SPM concentration in coastal zones.

Mackinnon et al. (1996) used MSS and GOES-VISSR and found that the 500 nm wavelength was good for determining SPM concentration, particularly in dust storm. Jacobberger et al.(1983) used the MSS data and found that the wavelength between 500 to 800 nm was best for the estimation of SPM concentration in coastal zone, whereas Zhu (2001) used MSS and TM data and mentioned that MSS-4 (800 nm - 1100 nm) and TM-4 (760 - 900 nm) was suitable for measuring outlines of water bodies.

2.4 Thematic Mapper (TM) Investigations

Several researchers used the TM band for the measurement of correlation coefficient between TM bands and SPM concentrations and found a curvilinear relationship between suspended sediments and radiance or reflectance (Ritchie et al. 1976, 1990, and Curran and Novo 1988).

It was demonstrated that TM bands 2 and 3 between wavelength 520 - 690 nm were best for the determination of SPM concentration in coastal zones. Other researchers mentioned that TM band 4 (760 - 900 nm) was better. For example, Thematic Mapper (TM) image containing a visible wavelength range (520 - 690 nm) was used to process data relating the reflectance along the water surface and light penetration by Mancebo et al. (1997). They found correlation coefficients between TM bands 2 and 3 and Total Suspended Sediments (TSS) to be 0.99 and 0.96, respectively.

Chen et al. (2004) derived the reflectance of TM bands 1 - 4 by using the COST method which expands on the DOS (Dark Object Subtraction) model. They found that TM bands 2 and 3 with the wavelength of 520 - 690 as being good for determining the reflectance of SPM concentration. Islam et al. (2001) estimated the suspended sediments from the reflectance of TM band 3 and found wavelength 630 - 690 nm was the best fit. Nellis et al. (1998) found that LANDSAT band 3 (630 - 690 nm) data have the best predictive ability of SPM in coastal areas. Lathrop (1992) used TM band 3 data and found it the best for estimation of suspended sediment concentration.

Different TM bands were preferred by different researchers according to the concentration of suspended sediments in shallow water zones. For example TM band 3 (630 - 690 nm) was preferred by Tassan (1987) for determination of suspended

particulate matter (SPM) concentration above 1mg/l. TM bands 2 and 3 (520 - 690 nm) for SPM concentrations between 5 - 50 mg/l, was found by Dekker et al. (2002) to be the best fit.

Topliss et al. (1990) mentioned that if SPM concentration was between 5-100 mg/l then TM bands 2 and 3 (520 - 690 nm) was good. You and Hou (1992) found that TM bands 2 and 3 (520 - 690 nm) were best for SPM concentration between 40-380 mg/l.

Ritchie et al. (1976, 1990) however preferred TM band 4 (700 - 800 nm) for SPM concentration between 30-200 mg/l. Tolk et al. (2000) stated that the bright bottom had the greatest impact at visible wavelengths. When suspended sediment concentrations exceeded 100 mg/l, the bright bottom response was found to be negligible and, substrate brightness has minimal impact between 740 and 900 nm, suggesting that this wavelength range was best for measuring suspended sediment concentrations.

Maktav et al. (2002) used LANDSAT-5 TM data and found that location and delineation of water bodies were clearly delineated using near-infrared wavelength due to its absorption properties.

2.5 Enhanced Thematic Mapper Plus (ETM+) Studies

The Enhanced Thematic Mapper Plus (ETM+) is now widely used in estimation of suspended sediment concentrations in water bodies. For example; Doxaran et al. (2002a, 2003, 2004a, 2004b) used LANDSAT ETM+ to locate the maximum turbidity zone and developed a relationship between near infrared and visible bands (NIR/VIS), and suspended sediment concentration.

Ouillon et al. (2004) performed different types of regression for ETM+ Band 1, 2 and 3 and for the band ratios, and found that the best fit result was between ETM+ Band 2 (from 525 nm to 605 nm) and turbidity averaged over the uppermost 5 m. He also found a linear regression relationship between LANDSAT 7 ETM+ Band 2 and above-water spectral reflectance.

Merry et al. (2006) used Landsat 7 to quantify suspended sediment concentrations in water bodies. A regression model was developed to quantify the suspended sediment concentrations at a sampling station with the corrected Landsat 7 ETM+ data. The results demonstrated a strong loglinear relationship between the suspended sediment concentration (and turbidity), and the visible green band (ETM+ Band 2) and the near infrared band (ETM+ Band 4).

Several remote sensing algorithms were compared by Wijekoon et al. (2006) to determine which was the most effective at identifying total suspended particulate in the western basin of Lake Erie. The results showed that a version of the normalized difference water index (NDWI), which retrieved reflected satellite data from the visible and short wave infrared spectral regions of the Landsat imagery, worked best as a mapping tool for suspended sediment plumes. This was because suspended sediment was found to be reflective in the visible wavelength region, while clear water was an efficient absorber in the near infrared part of the electromagnetic spectrum. The NDWI index values were found to be proportional to the concentration of suspended sediments in the water body.

CHAPTER 3

3.0 DATA ACQUISITION AND DATA PREPROCESSING

3.1 Acquisition of Landsat Data

To fulfill the objectives of this thesis, data from the LANDSAT MSS, TM and ETM+ sensors were utilized. The principal reason for using data from the LANDSAT satellites lies in the fact that the LANDSAT satellites provide the longest available sequence of remote sensing data on the continents and oceans of the world.

Data from four time periods were used. Images were acquired for May 1, 1985, September 19, 1992, October 9, 1999 and October 1, 2002. The May 1, 1985 data were from the MSS sensors and represent four spectral bands stretching from 0.5 micrometers to 1.1 micrometers (see Table 3.1a). The data for September 19, 1992 and October 9, 1999 time periods were from the Thematic Mapper, and represent seven spectral bands (see Table 3.1b). The October 1, 2002 data were from the ETM+ sensor with seven spectral bands stretching from 0.45 micrometers to 12.5 micrometers (see Table 3.1c).

Table 3.1a: MSS Bands

LANDSATs 4-5	Wavelength (micrometers)	Wavelength (nanometers)	Resolution (meters)
Band 1	0.5-0.6	500-600	82
Band 2	0.6-0.7	600-700	82
Band 3	0.7-0.8	700-800	82
Band 4	0.8-1.1	800-1100	82

Table 3.1b: TM Bands

Bands	Wavelength (micrometers)	Wavelength (nanometers)	Resolution (meters)
1	0.45-0.52	450-520	30
2	0.52-0.60	520-600	30
3	0.63-0.69	630-690	30
4	0.75-0.90	750-900	30
5	1.55-1.75	1550-1750	30
6	10.4-12.5	10400-12500	120
7	2.08-2.35	2080-2350	30

Table 3.1c: ETM+ Bands

Bands	Wavelength (micrometers)	Wavelength (nanometers)	Resolution (meters)
1	0.45-0.515	450-515	30
2	0.525-0.605	525-605	30
3	0.63-0.69	630-690	30
4	0.75-0.90	750-900	30
5	1.55-1.75	1550-1750	30
6	10.40-12.50	10400-12500	60
7	2.09-2.35	2090-2350	30

A remote sensing image is a numerical representation of radiance amplitudes from the surface. Each of the bands of the four images is composed of picture elements (pixels). The brightness value associated with each pixel is usually represented by a digital number (DN). DNs are positive integers that could range from 0 to 255.

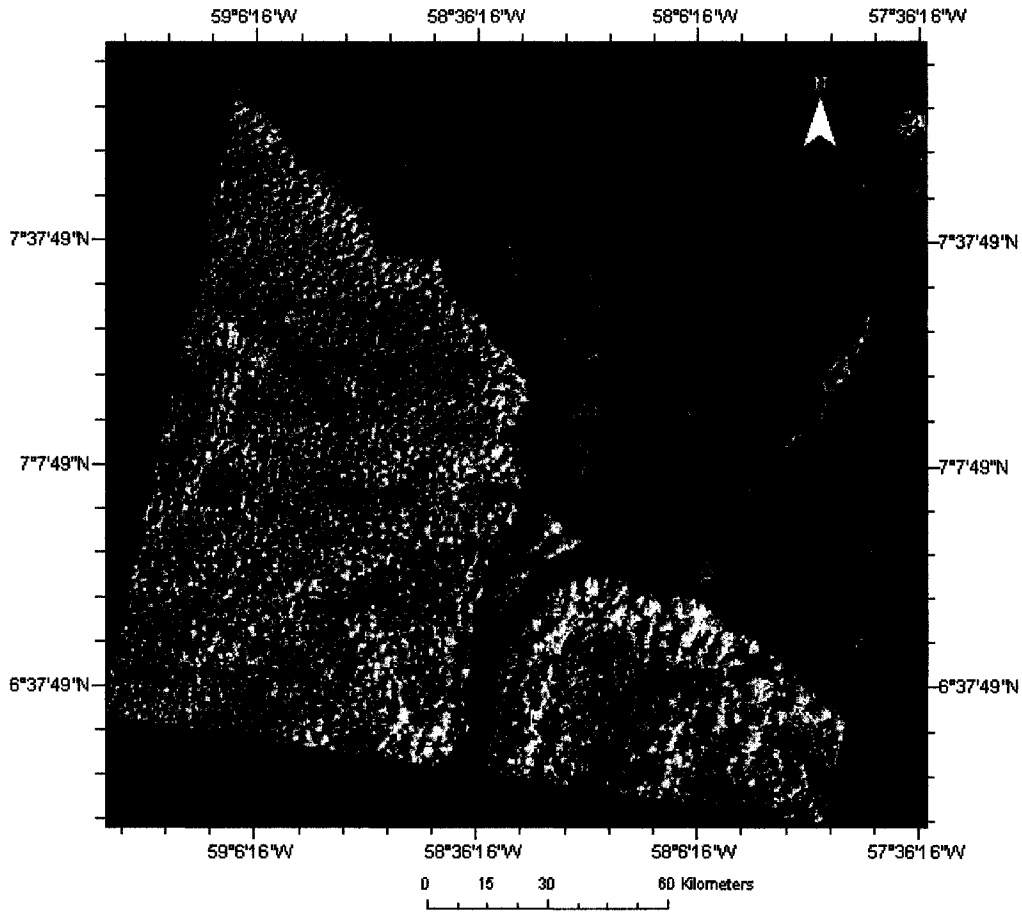

Figure 3.1: Remote Sensing Image of the Study Area

Data for each of the aforementioned time periods and for each band were obtained for a portion of the Demerara coast and the Essequibo coast. Figure 3.1 provides a remote sensing image of the delineated study area.

3.2 Data Preprocessing

Before the data for the four images were used it was necessary to perform several image processing functions in order to make the data useful for analysis with a geographical information system (GIS). Several image processing techniques

incorporated in the Idrisi Kilimanjaro version 14.002 software (Clark Labs, 2004) were utilized to process the images. In selecting appropriate image preprocessing techniques it was decided to follow the approach recommended by Lakhan (1993) who used remote sensing techniques to study wetlands along the Guyana coast. The techniques selected and described below required performing on each image geometric corrections, creation of a mask to separate land from water in each image, and plotting of image data to examine the distribution of DN values for each band.

3.3 Geometric Corrections

Raw digital images usually contain geometric distortions introduced by various factors ranging from variations in attitude, altitude, and velocity of the sensor platform. "The intent of geometric correction is to compensate for the distortions introduced by these factors so that the corrected image will have the geometric integrity of a map" (Lillesand and Kiefer, 1994, p. 528). In remote sensing applications, distortions are normally corrected by analyzing well-distributed ground control points (GCPs) occurring in an image.

After examining the metadata associated with each of the four images, it was decided to use the October 9, 1999 image as the base image for geometric correction. This is due to the fact that when importing the GeoTiff format for Landsat 7 ETM+ images into Idrisi no input is required from the user. The required information is already embedded in the image file. The geometric correction was done in Idrisi with the Resample module. A working folder for resampling was prepared because of the

requirements of the Idrisi software. Each image was located in its own folder within the working folder.

Composite images were then created for each image to better distinguish features on the ground. A composite image was first created for the October 9, 1999 image. Band 3 was selected for the blue image band, Band 4 for the green image band and Band 5 for the red image band. The composite image for 1999 is shown in Figure 3.2. Another composite image was created for the October 1, 2002 image. Bands 3, 4 and 5 were selected for the composite image for October 1, 2002. This composite image is shown in Figure 3.3.

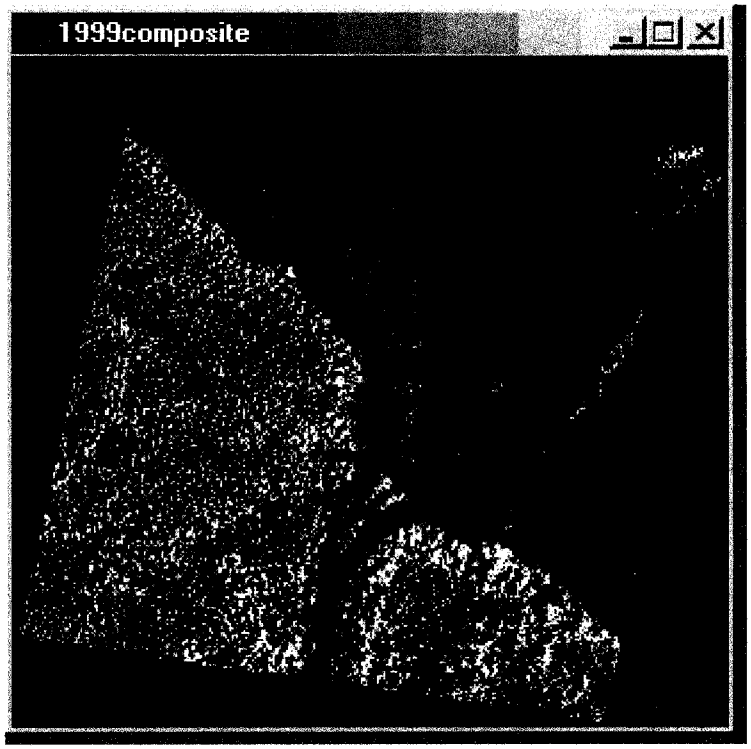

Figure 3.2: Composite Image Using Bands 3, 4 and 5 for the October 9, 1999 Landsat ETM+ Image

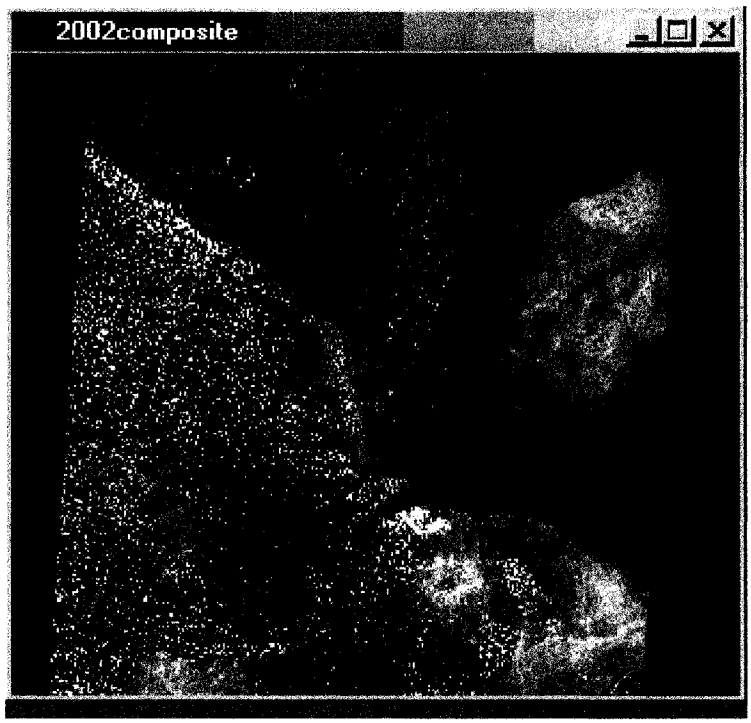

Figure 3.3: Composite Image Using Bands 3, 4 and 5 for the October 1, 2002 Landsat ETM+ Image

In the process of resampling the October 1, 2002 image to the October 1, 1999 image, the five bands for the 2002 image were grouped together as an RGF (raster group file). The 2002 composite image was used as the input reference, and the 1999 image was used as the output reference. GCPs were then placed on the input reference 2002 composite image.

To input the ground control points the mapping function chosen was Linear, and the resampling type chosen was Bilinear. Although the Linear mapping function required a minimum of three GCPs this study, after field investigations, chose a total of eighteen GCPs. These eighteen GCPs, distributed throughout the Landsat image area, were obtained by the author and his supervisor after extensive field work in Guyana.

Topographic map data, field markers, and global positioning system data were used to establish GCPs.

The first GCP was placed at the tip of the small island at the mouth of the Essequibo River. This GCP is shown in the 2002 image composite image and 1999 composite image (see Figure 3.4). The restored images with the first GCP are illustrated in Figure 3.5. It should be noted that the x and y coordinates for this control point are clearly indicated at the bottom of the images.

The second GCP was then located directly to the west of the small island which is the location of the first GCP. Figure 3.6 shows the relationship of the second GCP to the first GCP. The remaining sixteen GCPs were then registered. After inputting all eighteen GCPs (see Figure 3.7) the total RMS (root mean square error) was checked. Since the

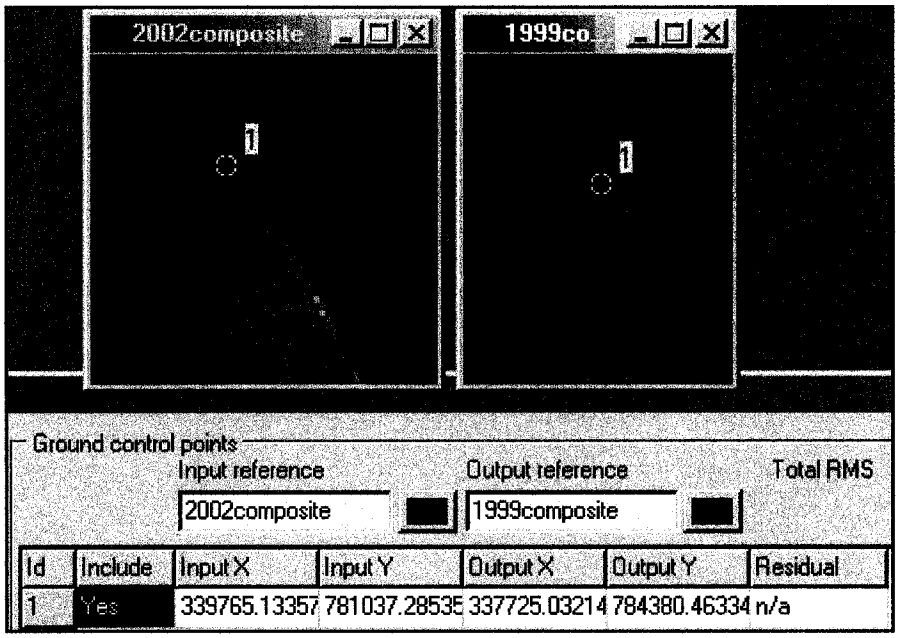

Figure 3.4: First Ground Control Point is Digitized

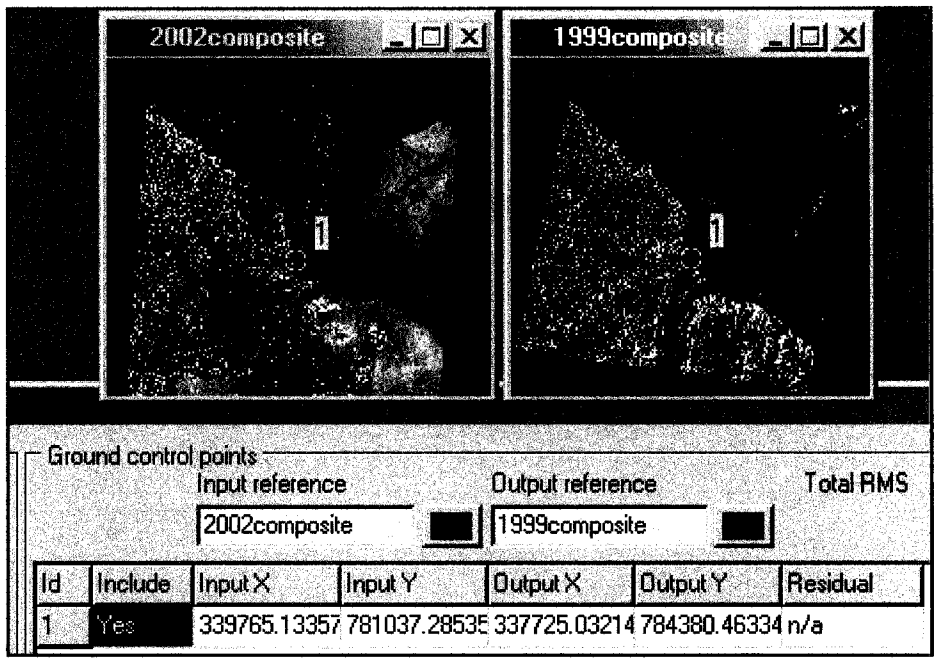

Figure 3.5: First Ground Control Point Shown in Both Images After Their Original Size is Restored

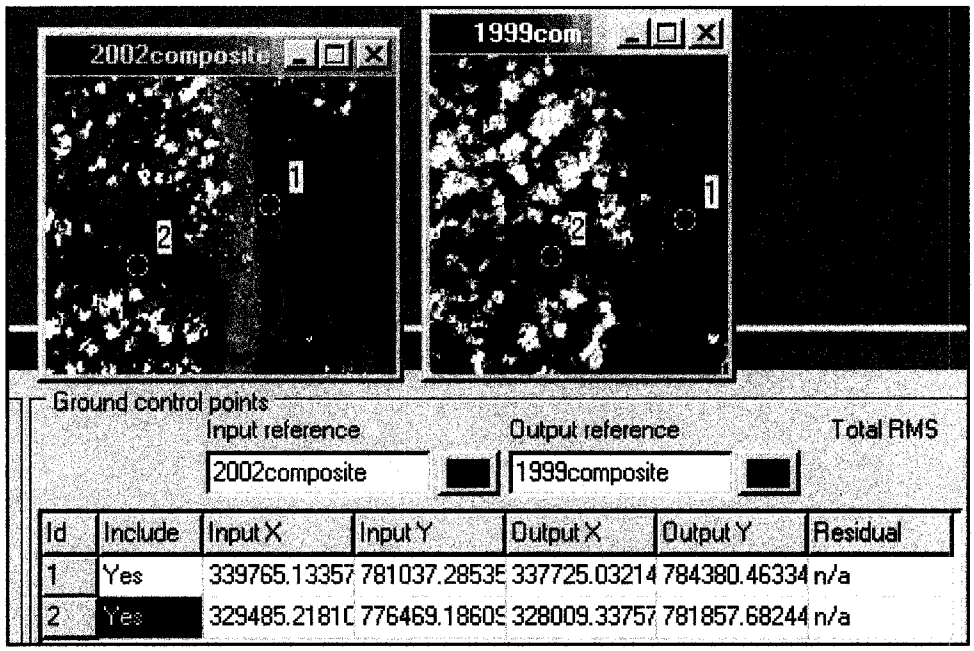

Figure 3.6: Ground Control Points 1 and 2 Shown in Both Images

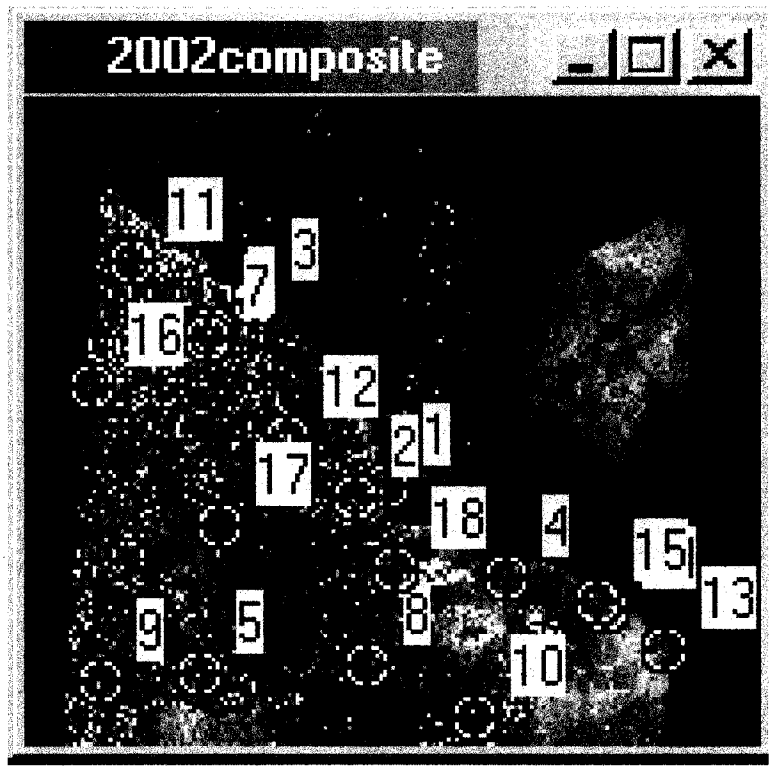

Figure 3.7: Landsat Image for October 1, 2002 Showing All 18 Ground Control Points (Some points (i.e., 14, 15 and 6, 7) overlap at the displayed scale).

Landsat images have a resolution of approximately 30 m, the total RMS error must be 15 m or less. As shown in Table 3.2, this was achieved because the RMS error was 7.19 m. Based on this very low RMS error, all four images were successfully rectified and referenced thereby permitting integration of the remote sensing images into a GIS database.

Table 3.2: Eighteen Ground Control Points - Total RMS Error is Only 7.190408 m.

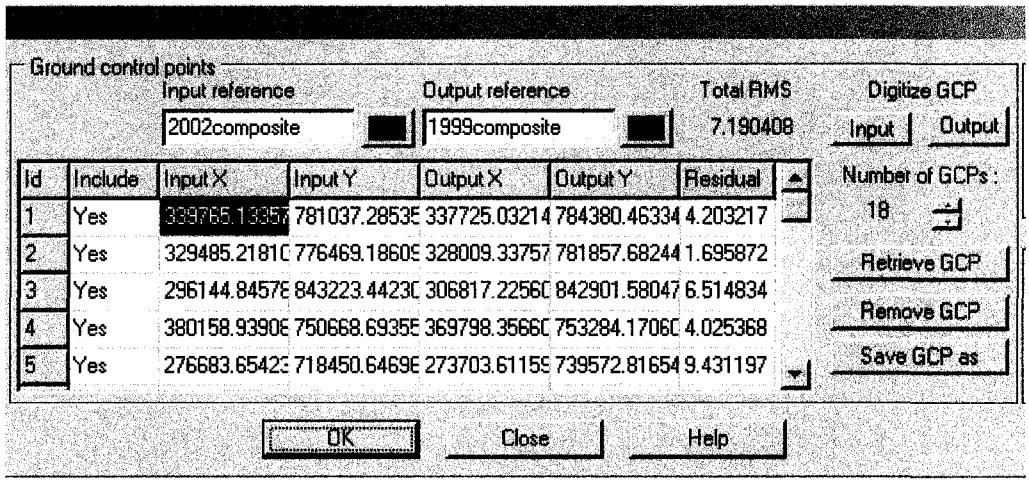

Id	Include	Input X	Input Y	Output X	Output Y	Residual
1	Yes	339765.13857	781037.28535	337725.03214	784380.46334	4.203217
2	Yes	329485.21810	776469.18605	328009.33757	781857.68244	1.695872
3	Yes	296144.84578	843223.44230	306817.22560	842901.58047	6.514834
4	Yes	380158.93908	750668.69355	369798.35660	753284.17060	4.025368
5	Yes	276683.65423	718450.64698	273703.61159	739572.81654	9.431197

3.4 Mask Creation to Separate Land from Water Areas

Following geometric corrections, it was necessary to create a mask file to mask out the land area in the Landsat image bands because this thesis focused on investigating suspended sediments in the coastal marine environment. The unavailability of the Idrisi add-on module, CartaLinx, which is normally used for masking purposes, necessitated the use of ArcMap. To aid in the task of digitizing a mask file a coastal dataset for the area of interest along coastal Guyana, representing the approximate area of the Landsat images, was downloaded from the ESRI World Base Map data (ESRI, 2006). The data were downloaded as a shapefile, and named ESRI_County_Areas_1. The advantage in using the downloaded shapefile was that the shapefile was in WGS 1984 coordinates which can then be projected to UTM coordinates for Zone 21N in ArcMap. The downloaded shapefile shows the counties along the coast of Guyana from near the Berbice River in the east to the Barima River in the west (see Figure 3.8).

Figure 3.8: Downloaded ESRI Shapefile as Displayed in ArcMap
Source: ESRI (2006)

3.4.1 Project Downloaded Shapefile to UTM Zone 21N Coordinates

In ArcMap, the shapefile was projected to UTM Zone 21N coordinates to match the Landsat image coordinate system which was also UTM Zone 21N. With the 1999 Landsat image considered as a reference image, Band 1 of the 1999 Landsat image was exported from Idrisi for addition to ArcMap. In ArcMap, the 1999 Band 1 raster image coincided closely along the coastal area with the projected shapefile. After resampling the image bands for 1992, 2002, and 1985 they were projected in Idrisi to UTM Zone 21N. Band 3 for 1985, Band 4 for 1992, and Band 3 for 2002 were exported from Idrisi as GeoTiff files to aid in mask creation in ArcMap.

3.4.2 Editing the Shapefile Using the 1999 Image and the Selected Projected 1985, 1992 and 2002 Image Files in ArcMap

The selected 1985, 1992, and 2002 Landsat GeoTiff raster files were added to ArcMap. Each of the images coincided with the 1999 image, although there were small land areas which required editing. ArcMap editing features were used to merge the polygons representing the counties to one large polygon. The editing features were also used to resize the polygon to coincide with the area of the 1999 Landsat image along the coast. After editing, a polygon was obtained that represented the same offshore areas for all four images. This polygon is illustrated in Figure 3.9. The file in ArcMap (Figure 3.9) was used as a basis for the creation of the land mask in Idrisi.

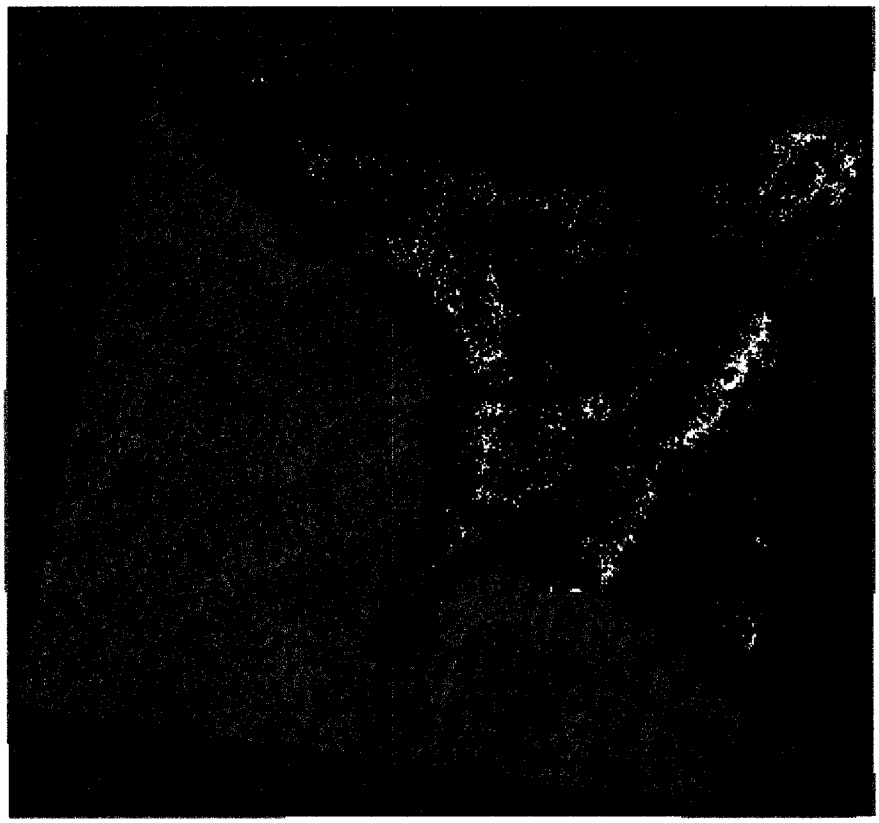

Figure 3.9: Final Polygon Used for Mask Created in ArcMap

3.4.3 Creating Mask File in Idrisi

The shapefile from ArcMap was imported to Idrisi and displayed. To create a raster image file in Idrisi from the imported vector file a vector to raster conversion was performed. In this conversion the land area was assigned the value of 1 and the offshore area was assigned the value of 0. Here it should be mentioned that these values were subsequently reversed. The created raster image file with land values specified as 1 is demonstrated in Figure 3.10.

Figure 3.10: Initial Mask Showing Land Values as 1

To reverse the values in the mask file the Image Calculator available from the GIS Analysis/Mathematical Operators menu was used. The land values were removed from the Landsat image bands with the Overlay operation. This Overlay operation was used to mask out the land areas for all the image bands namely, Bands 1-5 (2002), Bands 1-5 (1999), Bands 1-5 (1992) and Bands 1-4 (1985). Figure 3.11 illustrates, as an example, the image 2002_Band1 where all land values are 0 and the offshore water areas have their representative digital number (DN) values. Numeric histograms and line plots were then obtained for the DN values for each of the bands for all four images.

Figure 3.11: 2002 Band 1 Masked Showing Land Values in Black, and DN Values for Offshore Areas

3.5 Numeric Histogram and Line Plots of DN Values

To gain insights on the groupings and distributions of DN values in each band, numeric histogram data and line plots were produced. Idrisi's histogram module was used to produce numeric image histogram data for each of the bands for the four time periods. Table 3.3 provides an example of the numeric histogram data showing the frequency, minimum, maximum, and the mean for Band 1, 2002. The mean and standard deviation provide important clues on the concentration and variability of the DN values in the bands.

Table 3.3: Histogram of '2002_band1_masked' using 'mask_2_reverse' as mask

Class	Lower Limit	Upper Limit	Frequency	Prop.	Cum. Freq.	Cum. Prop.
3	51.000	68.000	5532	0.000	5532	0.000
4	68.000	85.000	2362557	0.042	2368089	0.042
5	85.000	102.000	6167591	0.109	8535680	0.151
6	102.00	119.000	3155986	0.056	11691666	0.207
7	119.000	136.000	1781214	0.032	13472880	0.239
8	136.000	153.000	1318060	0.023	14790940	0.262
9	153.000	170.000	1068436	0.019	15859376	0.281
10	170.000	187.000	900066	0.016	16759442	0.297
11	187.000	204.000	843553	0.015	17602996	0.312
12	204.000	221.000	671399	0.012	18274396	0.324
13	221.000	238.000	443407	0.008	18717804	0.331
14	238.000	255.000	261544	0.005	18979348	0.336
	Values > max. specified		37357453	0.662	56336800	0.998

Class width	=	17.000
Display minimum	=	0.000
Display maximum	=	255.000
Actual minimum	=	0.000
Actual maximum	=	255.000
Mean	=	123.475(based on 19113899 values within range (out of
Stand. Deviation	=	46.166 564713521)
df	=	19113898

The numeric histogram data were saved as a text file, and subsequently imported to Microsoft Excel. Each Landsat image was assigned its own worksheet in Excel. Line plots were then produced for each Landsat image showing the DN frequency versus the DN classes. From the line plots (Figure 3.12, Figure 3.13, Figure 3.14, and Figure 3.15) the frequency and distribution of the digital numbers in each of the bands could be determined. While Band 1 proved to be significant in each of the four images, no definitive conclusion could be made on the distinctiveness of any of the bands for discriminating sediment concentrations. In the 1985 image, most of the DN values were concentrated in the range 0 and 68 while in the 1992 image there were three broad areas of sediment concentration representing Bands 1, 2 and 3. In the 1999 and 2002 images all the bands contributed to the distribution of digital number values. Patterns demonstrating definitive clusters were difficult to ascertain.

Since the numeric histogram data and the line plots did not reveal clear separability in the information presented in the various bands for each of the time periods the decision was made to statistically extract relevant bands from each of the images. This must be done to facilitate integration of relevant bands in each image in the GIS. In addition, it is necessary to meet one of the objectives of this thesis and find the most appropriate bands reflecting suspended sediments.

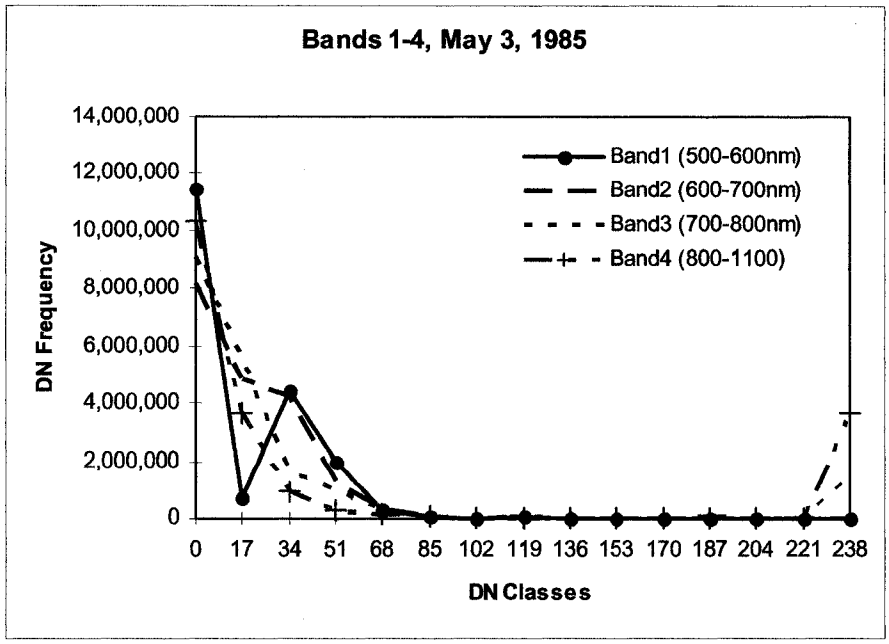

Figure 3.12: Line Plot of DN Values for MSS Data

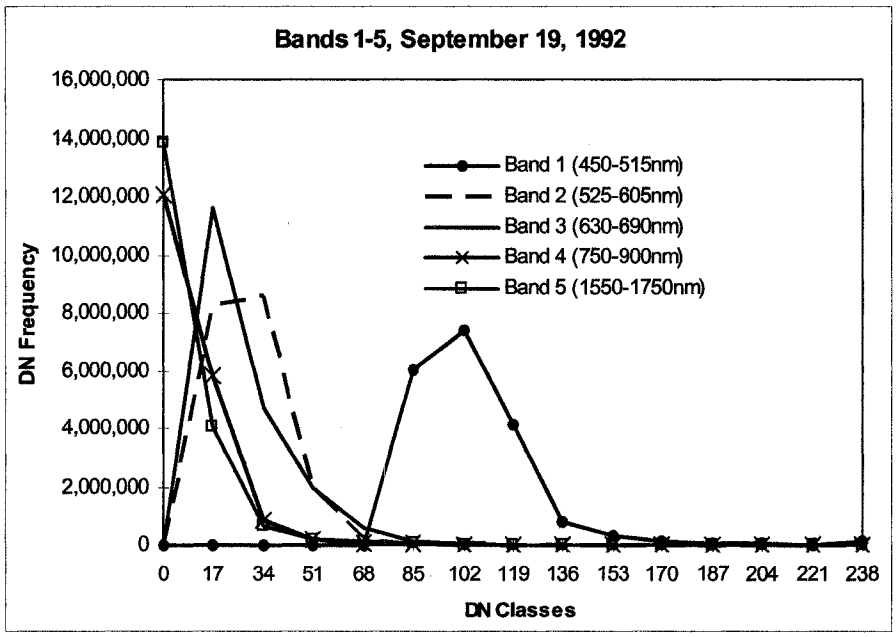

Figure 3.13: Line Plot of DN Values for TM Data

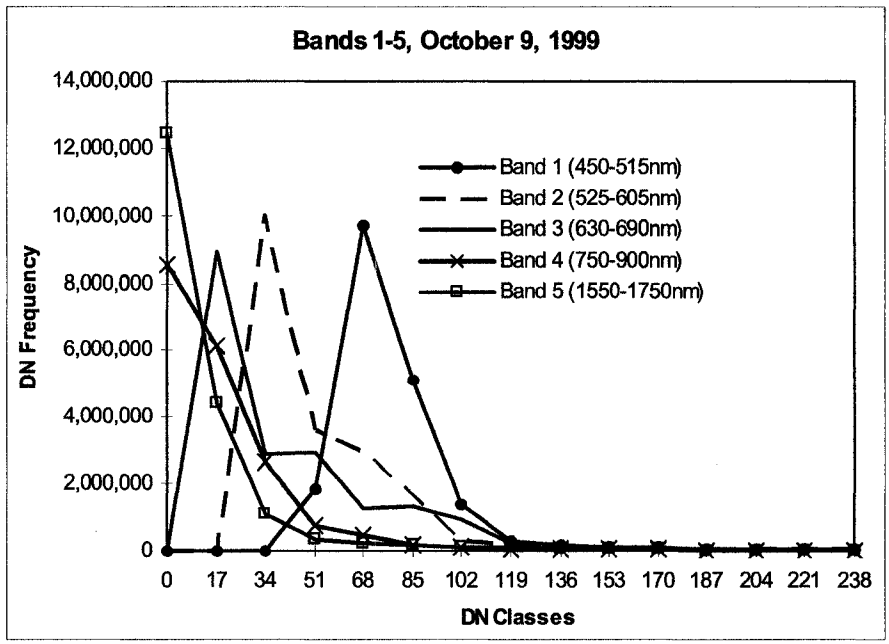

Figure 3.14: Line Plot of DN Values for ETM+ Data

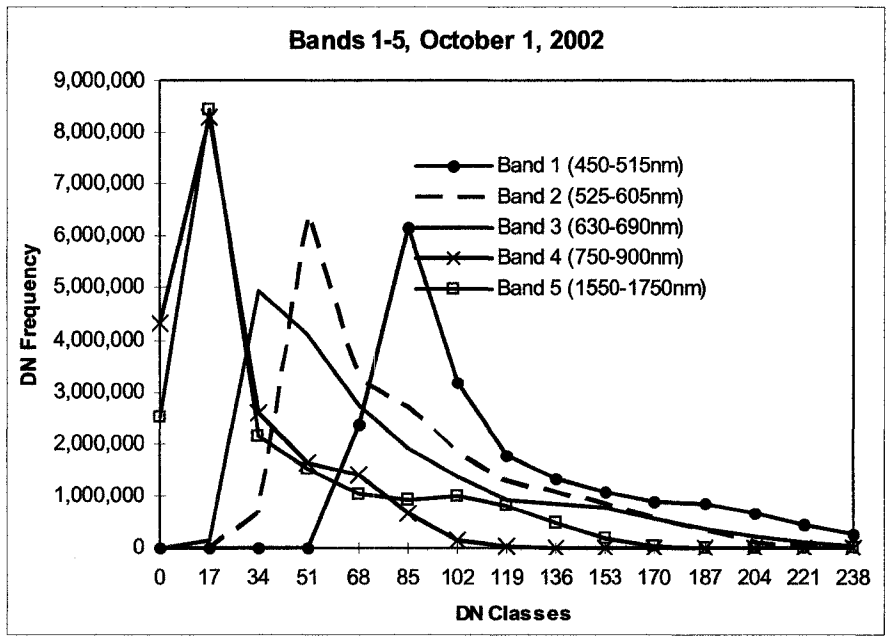

Figure 3.15: Line Plot of DN Values for ETM+ Data

CHAPTER 4

4.0 STATISTICAL ANALYSIS OF IMAGE DATA

4.1 Use of Principal Components Analysis

In order to identify appropriate spectral bands representing sediment concentrations, and assess the spatial patterns of sediment concentrations in the near and offshore waters the decision was made to extract statistically significant bands from each of the four images. The statistical technique of principal components analysis (PCA) was chosen because it was found by investigators (for example, Jensen, 1986; Jolliffe, 2002) to be applicable for reducing data present in multiple datasets. Lakhan (1993), who utilized principal component analysis to discriminate wetlands along coastal Guyana, reported that the technique is useful for producing a new set of images which are close approximations to the original set of images from which they were derived. Essentially, PCA is a decorrelation procedure that reorganizes by statistical procedures the DN values from the various spectral bands. The primary objective is to produce a new average image which will explain more of the total variance than could be done by one image. This objective is achieved through a correlation matrix which is created with all the standardized image data (Jolliffe, 2002). The sum of the correlations for each image is then found in order to check the similarity of the correlated image with all of the other images.

4.2 Results from Principal Components Analysis

Principal components analysis was performed with the Idrisi software utilizing the data from each of the spectral bands for all of the four datasets (1985, 1992, 1999 and 2002). The outputs from the principal components analysis consisted of a variance/covariance matrix, a correlation matrix, the components and associated eigenvalues and eigenvectors, and the component loadings. Table 4.1 provides an example of the output results from the 1985 image data. The variance/covariance matrix and the correlation matrix facilitate an understanding of the relationship between the various bands. The component summary which includes eigenvectors indicate the reverse

Table 4.1: Output From PCA Module for 1985 Image Bands

VAR/COVAR	1985_band1_masked	1985_band2_masked	1985_band3_masked	1985_band4_masked
1985_band1_masked	373.32	141.77	216.11	319.27
1985_band2_masked	141.77	345.34	224.31	343.43
1985_band3_masked	216.11	224.31	1747.99	173.79
1985_band4_masked	319.27	343.43	173.79	3941.52

COR MATRIX	1985_band1_masked	1985_band2_masked	1985_band3_masked	1985_band4_masked
1985_band1_masked	1.000000	0.394829	0.267530	0.263204
1985_band2_masked	0.394829	1.000000	0.288708	0.294361
1985_band3_masked	0.267530	0.288708	1.000000	0.066209
1985_band4_masked	0.263204	0.294361	0.066209	1.000000

COMPONENT	C1	C2	C3	C4
% var.	45.28	23.35	16.45	14.92
Eigenval.	1.81	0.93	0.66	0.60
Eigvec.1	0.557008	-0.011068	-0.655741	-0.509533
Eigvec.2	0.575386	0.010315	-0.137807	0.806123
Eigvec.3	0.423001	-0.707557	0.528607	-0.202506
Eigvec.4	0.423961	0.706495	0.521141	-0.222562

LOADING	C1	C2	C3	C4
1985_band1_masked	0.749659	-0.010695	-0.531973	-0.393576
1985_band2_masked	0.774393	0.009968	-0.111797	0.622669
1985_band3_masked	0.569303	-0.683760	0.428835	-0.156421
1985_band4_masked	0.570596	0.682733	0.422779	-0.171913

transformation necessary to return the component back to its original DN values for each band. When the eigenvectors for the first principal component are squared then the proportion of the variance explained by each band in the principal component is highlighted. The eigenvalues express the amount of variance explained by each component.

The most important information from the principal components output is the component loadings. In brief, the component loadings are the degree of correlation between the new components and the original bands. The component loadings for each band for each of the four image years are presented in Table 4.2. When these component loadings are examined it could be seen that Band 2 for 1985 has the highest component loading for component 1 (C1). For this reason, Band 2 for the 1985 image (Figure 4.1) was used for integration in the GIS database. The component loadings in Table 4.2 also demonstrated that Band 3 for the 1992 image has the highest loadings for C1. Therefore, Band 3 for the 1992 image (Figure 4.2) was chosen for GIS image integration. The PCA results for the 1999 and 2002 images were examined in a similar manner. In both cases, C1 explained the most variance in each image for each year. The component loadings for the 1999 image showed that Bands 2, 3 and 4 have significant loadings. The component loadings for the 2002 image demonstrated that Bands 3, 2, and 4 contributed the most to the component loadings. Since only small differences existed in the component loading values, Band 2 for the 1999 image (Figure 4.3), and Band 3 for the 2002 image (Figure 4.4) were selected for integration and analysis by the GIS. These selected bands provide

invaluable information on the association of specific spectral bands with correlation of suspended sediments.

Table 4.2: Summary of Component Loadings

Spectral Bands	Component 1	Component 2	Component 3	Component 4	Component 5
MSS Band 1, 1985	0.750	-0.011	-0.532	-0.394	N/A
MSS Band 2, 1985	0.774	0.010	-0.112	0.623	N/A
MSS Band 3, 1985	0.569	-0.684	0.429	-0.156	N/A
MSS Band 4, 1985	0.571	0.683	0.423	-0.172	N/A
TM Band 1, 1992	0.948	-0.284	-0.131	-0.046	-0.022
TM Band 2, 1992	0.981	-0.183	0.011	0.043	0.049
TM Band 3, 1992	0.986	-0.062	0.135	0.059	-0.034
TM Band 4, 1992	0.974	0.179	0.092	-0.101	0.009
TM Band 5, 1992	0.922	0.365	-0.119	0.045	-0.003
ETM+ Band 1, 1999	0.955	-0.234	-0.175	-0.054	-0.020
ETM+ Band 2, 1999	0.986	-0.159	-0.004	0.030	0.042
ETM+ Band 3, 1999	0.976	-0.103	0.168	0.090	-0.023
ETM+ Band 4, 1999	0.970	0.161	0.129	-0.127	0.002
ETM+ Band 5, 1999	0.925	0.352	-0.128	0.062	-0.002
ETM+ Band 1, 2002	0.973	-0.208	0.096	-0.012	-0.018
ETM+ Band 2, 2002	0.989	-0.124	-0.048	0.231	0.048
ETM+ Band 3, 2002	0.994	-0.021	-0.100	0.013	-0.041
ETM+ Band 4, 2002	0.987	0.139	-0.004	-0.077	0.010
ETM+ Band 5, 2002	0.973	0.214	0.058	0.053	-0.001

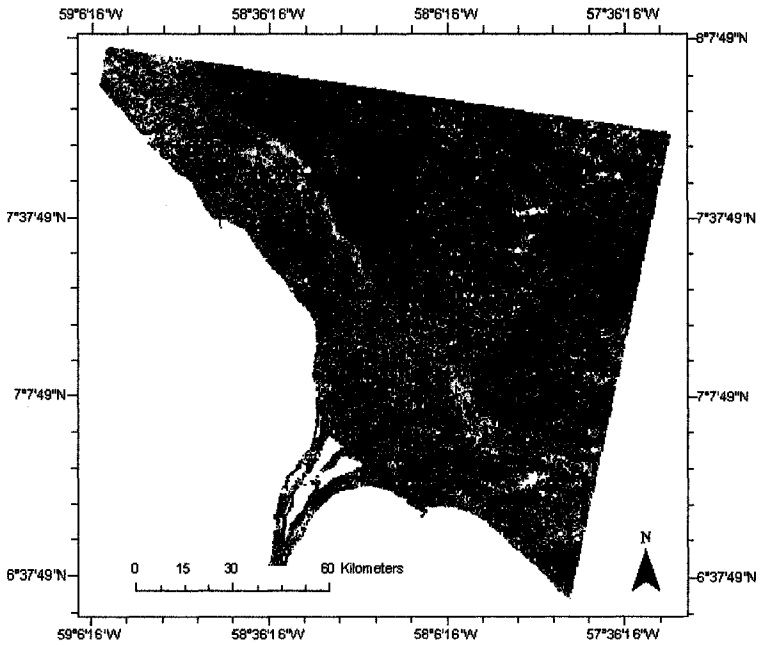

Figure 4.1: Band 2, 1985 Greyscale Image

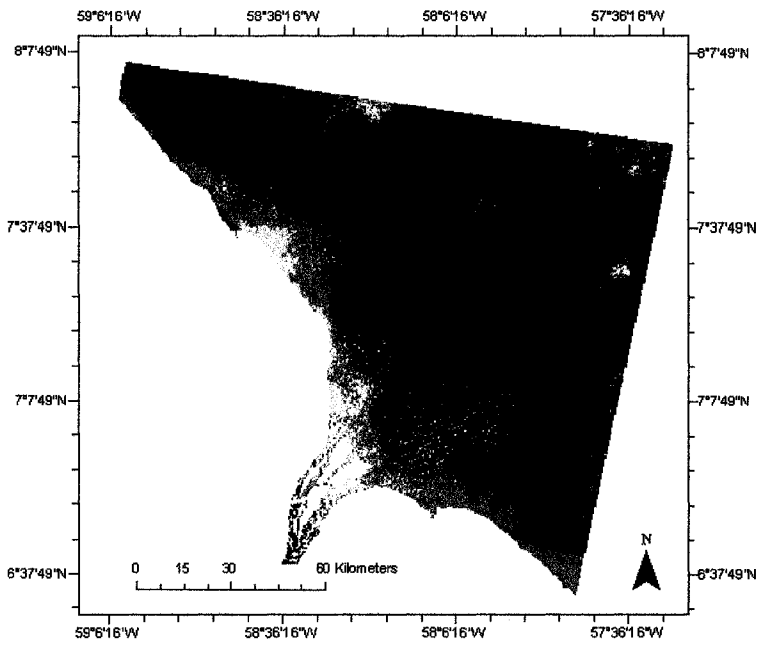

Figure 4.2: Band 3, 1992 Greyscale Image

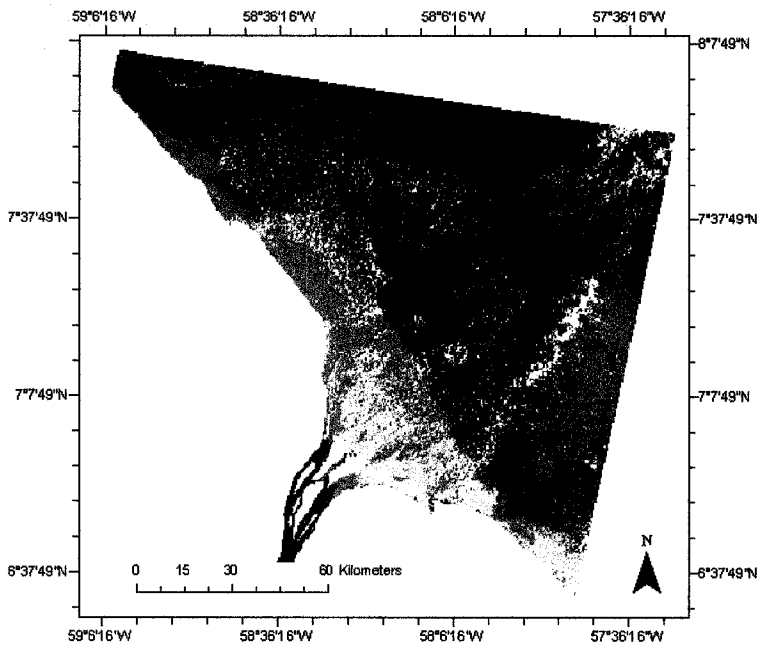

Figure 4.3: Band 2, 1999 Greyscale Image

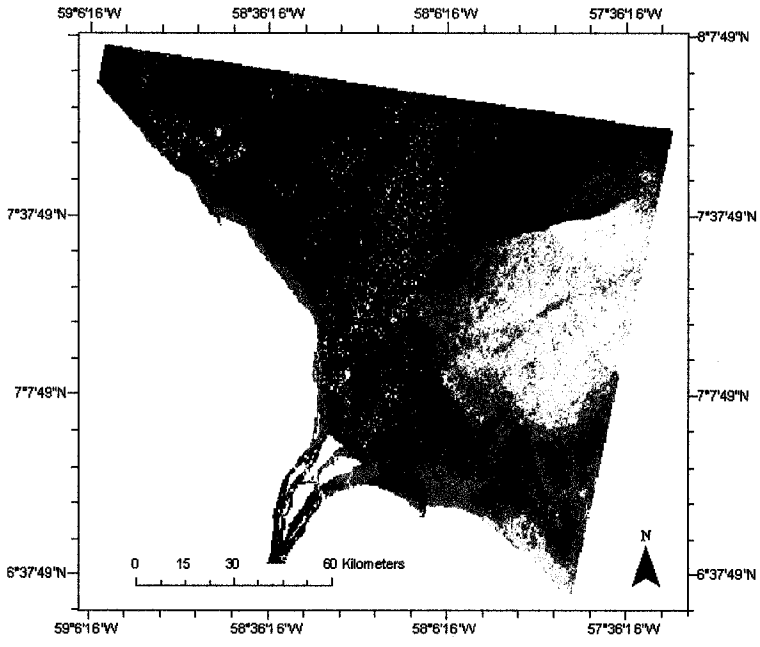

Figure 4.4: Band 3, 2002 Greyscale Image

CHAPTER 5

5.0 GIS DIGITIZATION OF SEDIMENT CLASSES

5.1 Selection of Sediment Classes

The PCA results for Band 2, 1985, Band 3, 1992, Band 2, 1999 and Band 3, 2002 were used as inputs to ArcGIS to express the distributions and different classes of suspended sediments in the near and offshore areas of the coastal zone. Since it has been established that higher concentrations of suspended sediments in water bodies cause an increase in the reflection from the surface water (Ritchie et al., 1976; Doxaran et al., 2002b), there is a strong association between higher digital number values and higher suspended sediment concentrations.

After examining the PCA images for 1985, 1992, 1999 and 2002 the decision was made to use four classes to represent the digital numbers associated with the masked images. In classifying the images in Idrisi, the quantiles autoscaling option was selected. Quantiles was chosen because it provided the closest approximation of the sediment bands visible in the PCA images. The classes selected are illustrated by the 1985 image (Figure 5.1), 1992 image (Figure 5.2), 1999 image (Figure 5.3) and 2002 image (Figure 5.4). Each of the images was represented with four classes of sediments. Here it should be emphasized that each class is associated with an area representing a different level of sediment concentration.

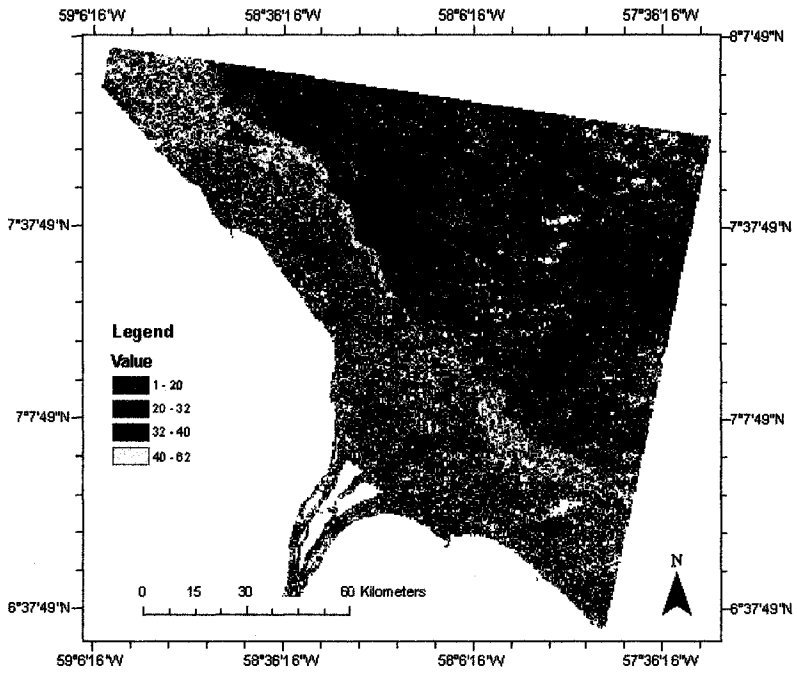

Figure 5.1: Classified Image for Band 2, 1985

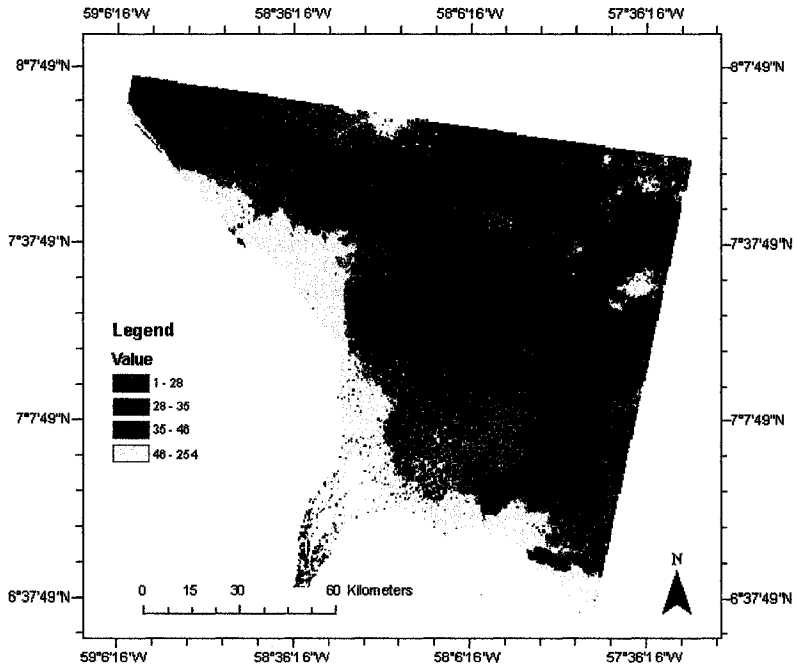

Figure 5.2: Classified Image for Band 3, 1992

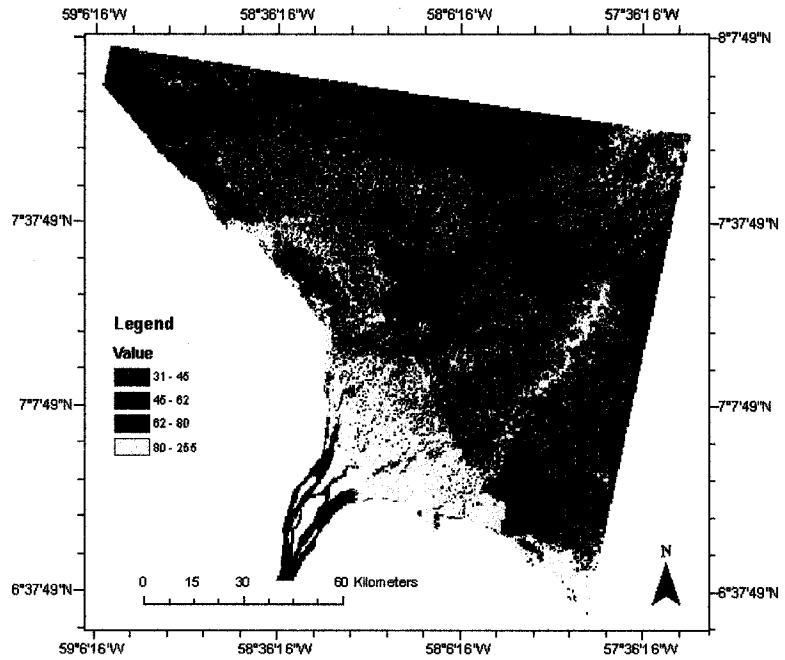

Figure 5.3: Classified Image for Band 2, 1999

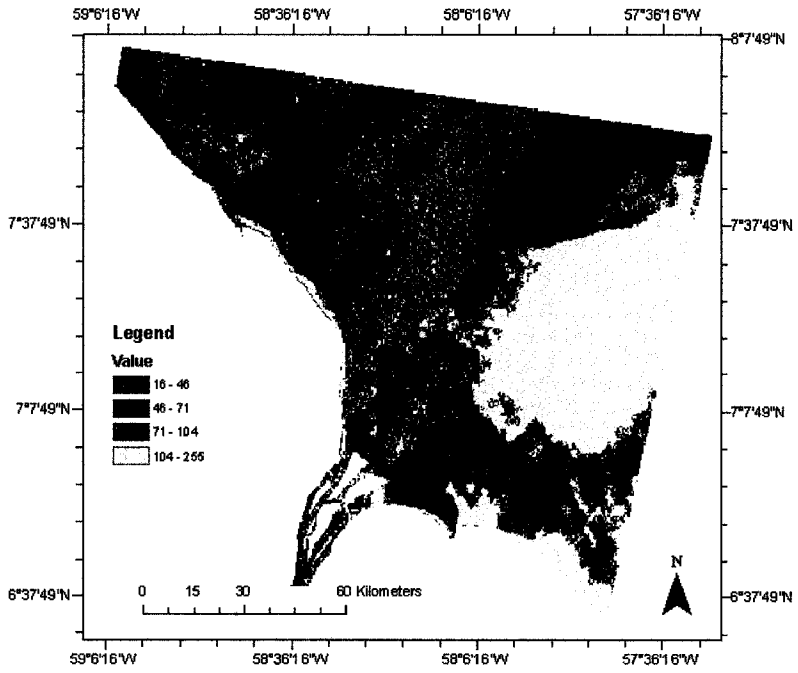

Figure 5.4: Classified Image for Band 3, 2002

5.2 Digitizing of Sediment Classes in ArcMap

The polygons representing the various classes of sediments in each of the images were then digitized in ArcMap. To perform digitizing in ArcMap the map file used to create the land mask layer was opened. The advantage in doing this is that subsequent layers or images added to the map file are displayed in the same geographic coordinates as the first layer in the file, namely the already created mask layer. Each of the images in ArcMap was carefully examined, and distinguishable polygons were digitized to represent the broad areas of suspended sediments shown in each of the four classified images.

The digitized sediment polygons for the 1985 image are shown in Figure 5.5. The DN range of 1-20 represent areas of low sediment concentration, and the DN range between 40 and 62 was considered as areas with high sediment concentrations.

In the 1992 image the polygons selected for digitization present a broad picture of sediment concentration in the coastal zone. It was determined that the brightest class would be with DN values between 46 and 254. After analysis of the DN values it was observed that DN values greater than 75 represented clouded regions, therefore this class was reduced to 46-75. The large area offshore was classified as having a DN range of between 1 and 28 because of the presence of light and grayish clouds on the satellite image. The two remaining polygons were distinguished as having DN range values of between 28 and 35, and 35 and 46. The digitized map with the sediment polygons is illustrated in Figure 5.6.

In the 1999 image it was determined that most of the large area in the far offshore region was covered by clouds ranging from the very visible white clouds to dark gray

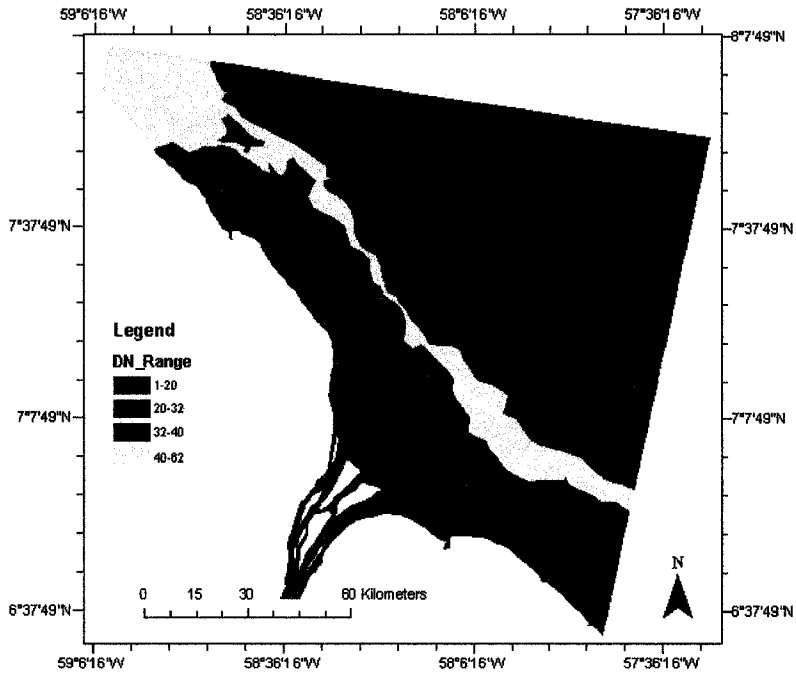

Figure 5.5: Sediment Polygons for Band 2, 1985

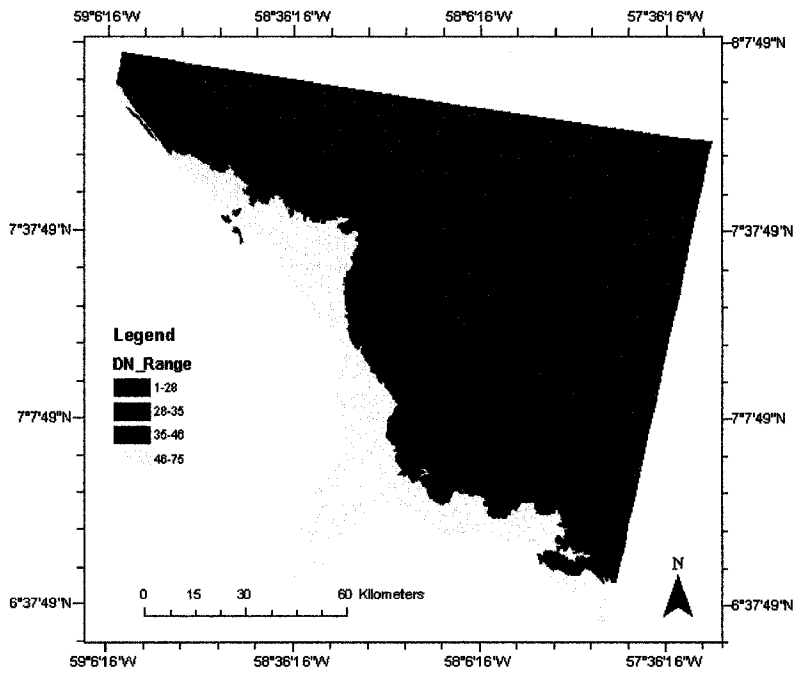

Figure 5.6: Sediment Polygons for Band 3, 1992

clouds with lower DN values. A large portion of the bright region was associated with DN values ranging from 31 to 45. For this reason most of the far offshore region was classified as having a DN range of 31 to 45. Areas with DN values ranging between 46 and 62 and 62 to 80 were representative of high concentrations of sediment. The area between 46 and 62 was almost similar to the broad band of sediment concentrations observed in the 1985 and 1992 images. Most of the sediments were concentrated in the nearshore area with DN values of between 80 and 100 (see Figure 5.7).

After examination of the classification ranges in the 2002 image, it was determined that the DN range of 16 to 46 was associated with a minimal amount of sediment. The maximum amount of sediment was in the small elongated area near to the shore with DN values ranging between 104 and 130. The areas with lesser amount of sediments had DN ranges of between 46 and 71 and 71 to 104. The very wide pattern of sediment concentration with DN values between 46 and 71 could be clearly seen in the digitized sediment map (Figure 5.8).

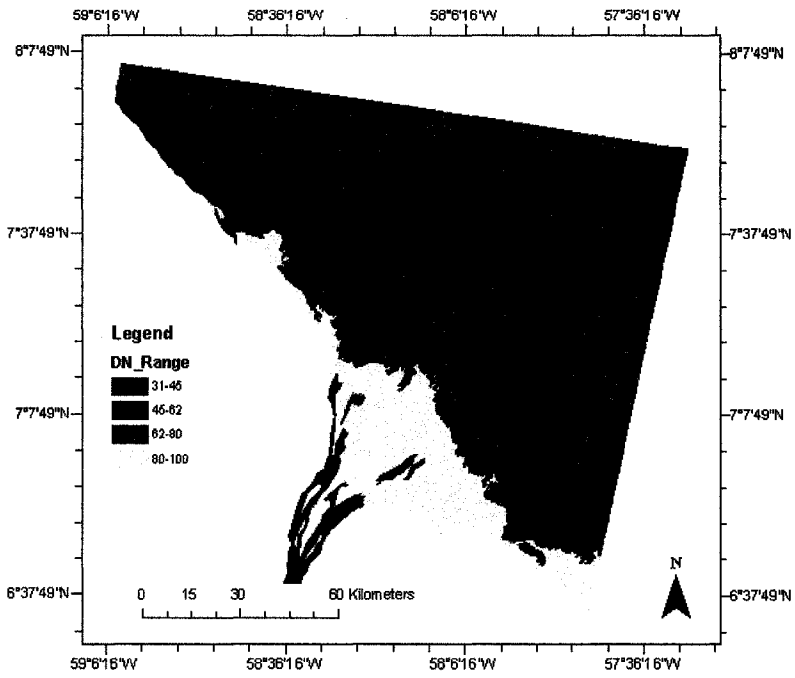

Figure 5.7: Sediment Polygons for Band 2, 1999

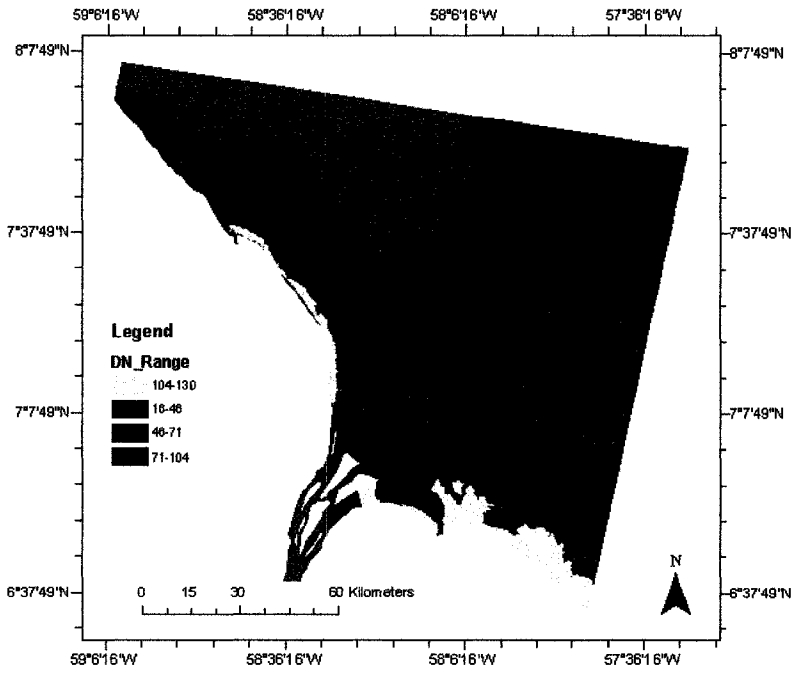

Figure 5.8: Sediment Polygons for Band 3, 2002

CHAPTER 6

6.0 GIS ANALYSIS AND RESULTS ON SEDIMENT CHANGES

6.1 Determining Areas of Change for Suspended Sediments

After polygons representing suspended sediments were digitized and classified for each year (1985, 1992, 1999 and 2002), it was decided to convert the feature classes to raster images in order to calculate differences in the images. The differences in the images will permit an assessment of whether there were positive (i.e., gains) or negative (i.e., losses) changes in sediments in the coastal environment during the 1985-2002 period. Before this was done, a common classification was devised for the four images (1985, 1992, 1999 and 2002) images.

6.1.1 Common Classification Scheme

Each image was classified with four classes associated with digital number (DN) ranges in the image. Therefore, there were a total of 16 classes among the four images. These classes were as follows:

	DN Range	Image Year
1)	1-20	1985
2)	1-28	1992
3)	16-46	2002
4)	20-32	1985
5)	28-35	1992
6)	31-45	1999
7)	32-40	1985
8)	35-46	1992
9)	40-62	1985
10)	45-62	1992
11)	46-71	2002

12)	46-75	1992
13)	62-80	1999
14)	71-104	2002
15)	80-100	1999
16)	104-130	2002

Upon examination of the 16 classes it was decided to use an approximate classification as follows:

DN Range	Class
1-20	1
20-40	2
40-60	3
60-80	4
80-100	5
100-130	6

Therefore, the 1985 image was reclassified with the following classes:

Old Class	DN Range	New Class	New DN Range
1	1-20	1	1-20
2	20-32	2	20-40
3	32-40	2	20-40
4	40-62	3	40-60

The 1992 image was reclassified with the following classes:

Old Class	DN Range	New Class	New DN Range
1	1-28	1	1-20
2	28-35	2	20-40
3	35-46	2	20-40
4	46-75	3	40-60

The 1999 image was reclassified with the following classes:

Old Class	DN Range	New Class	New DN Range
1	31-45	2	20-40
2	46-62	3	40-60
3	62-80	4	60-80
4	80-100	5	80-100

The 2002 image was reclassified with the following classes:

Old Class	DN Range	New Class	New DN Range
1	16-46	2	20-40
2	46-71	3	40-60
3	71-104	5	80-100
4	104-130	6	104-130

ArcCatalog was used to add the new fields to the attribute tables for the four images. In ArcMap, for each year, the previously saved map file was opened, and an editing session was started. The new class and DN range values were added to the feature attribute table using the Field Calculator window.

6.1.2 Raster Image Conversion

For each year, the digitized polygon feature class was converted to a raster image. Feature to Raster was used from the ArcToolbox. A legend was added to each new raster image showing regions representing suspended sediment associated with the DN Range off the coast of Guyana using a classification scheme that is common to all four images. An examination of Figures 6.1, 6.2, 6.3 and 6.4 demonstrate that the 1985 and 1992 images have lower DN Ranges than the images for 1999 and 2002.

The 1985 and 1992 have the lowest DN Ranges (Classes 1 to 3) of the four images. As mentioned previously, it was assumed that digital number values were associated with the presence or absence of suspended sediments in the image. A high DN indicated high reflectance in the image. The higher reflectance values in an image was

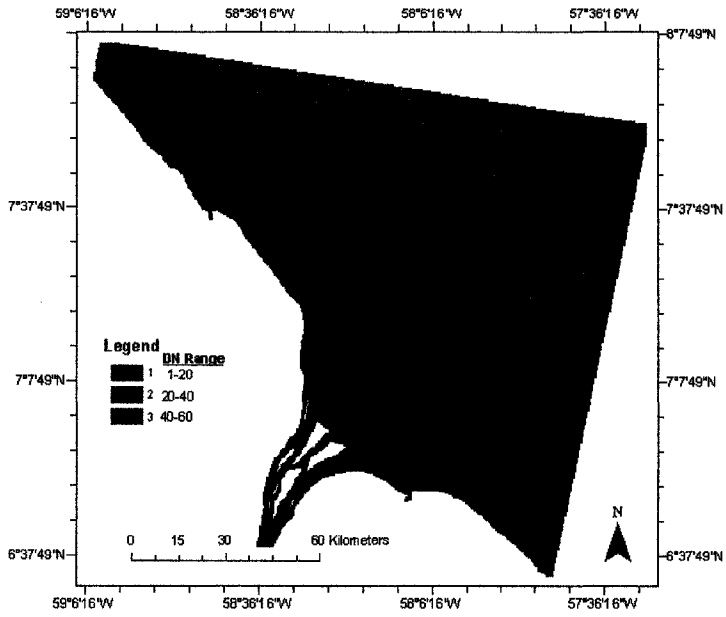

Figure 6.1: Band 2, 1985 as a Raster Image Showing Common Classification Scheme

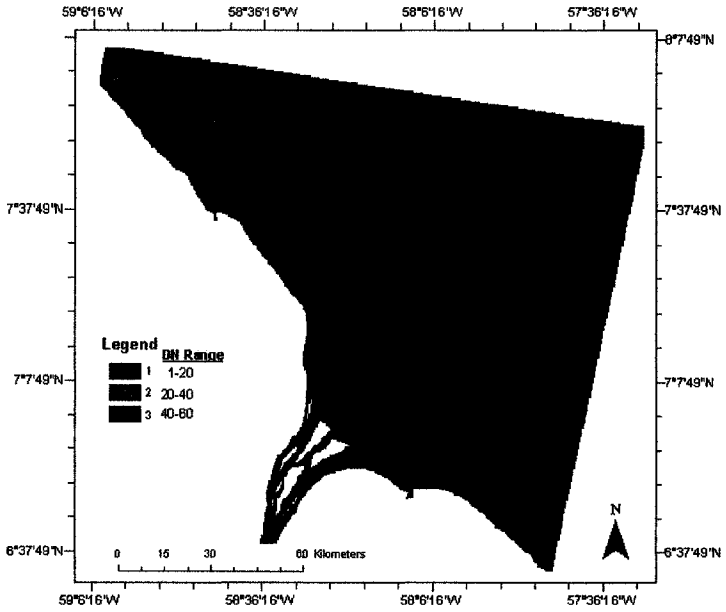

Figure 6.2: Band 3, 1992 as a Raster Image Showing Common Classification Scheme

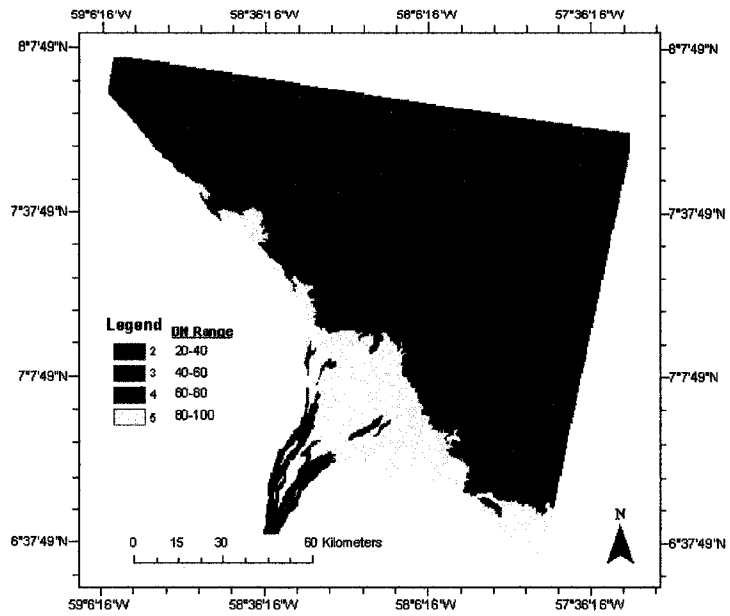

Figure 6.3: Band 2, 1999 as a Raster Image Showing Common Classification Scheme

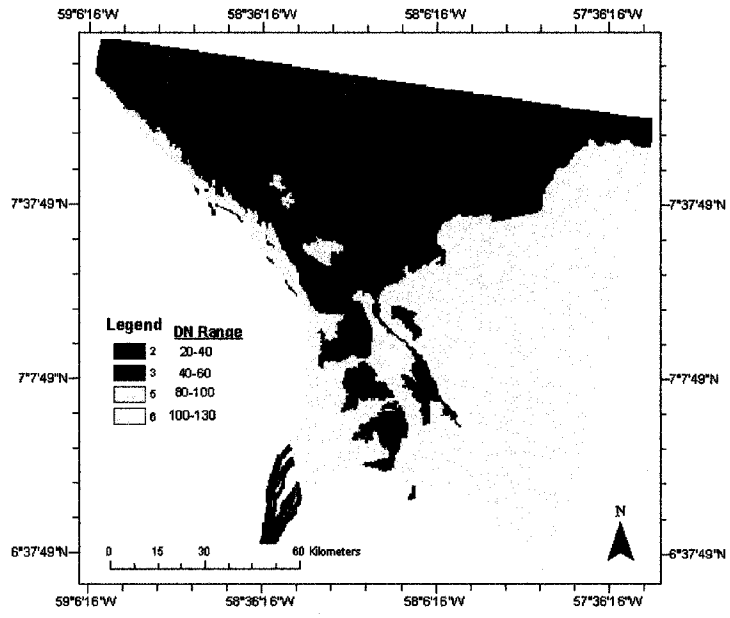

Figure 6.4: Band 3, 2002 as a Raster Image Showing Common Classification Scheme

associated with the presence of higher suspended sediment concentrations. Lower reflectance values would indicate the presence of comparatively less suspended sediments.

6.2 The Presence of Sediments Reflected by the 1985 and 1992 Images

Upon examination of the images for 1985 and 1992, it could be noted that the highest DN Range was Class 3 (40-60) for both images. Class 3 represented the narrow band in the coastal area approximately 30 km from land. The greatest concentration of sediment was, therefore, deemed to be Class 3 (DN Range 40-60), the narrow band approximately 30 km offshore.

In contrast, the 1992 image (Figure 6.2) showed that the three DN Ranges increased toward the offshore region. Offshore values had DN Range 40-60 (Class 3) whereas deeper water areas had DN Range 1-20 (Class 1). DN Range 40-60 (Class 3) was directly along the coast and was substantially reduced in the extreme northwest coastal area. Class 3 would, therefore, represent the area of greatest concentration of sediments for 1992.

6.3 The Presence of Sediments Reflected by the 1999 and 2002 Images

Both the 1999 and 2002 images have higher DN Ranges. Class 2 represented reflectance values between 20 and 40. Class 5 (DN Range 80-100) was directly along the coast except for the northwest corner of the image which had Classes 4 (DN Range 60-

80) and 3 (DN Range 40-60). Class 3 constituted a narrow band approximately 30 km offshore.

In contrast, in Figure 6.4 DN Ranges as high as 100-130 (Class 6) could be seen. These values were located offshore in the southeast corner of the image. It could be seen that Class 5 (DN Range 80-100) represented the largest are of sediment concentration and extended along the coastline from near Georgetown to the northwest corner of the image. The lowest DN Range (20-40; Class 2) was associated with the least sediment concentration, and was located in deeper water in the north and northwest corner of the image.

6.4 Image Differentiation

Image differentiation involved subtracting an earlier image from a later image. Image differentiation and associated percentage changes were performed using the Raster Calculator in Spatial Analyst. Image difference calculations were made for the four image periods, namely between 1992 and 1985, 1999 and 1985, 2002 and 1999, and 2002 and 1985.

6.4.1 Image Differencing Between the 1992 and 1985 Images

It could be seen from Figures 6.1 and 6.2 that both the 1985 and 1992 images have 3 DN Ranges (i.e., 1, 2 and 3) representing approximate DN Ranges from 1 to 60. From Figure 6.1 the brightest DN Range (approximately 40-60), represented the highest reflectance values in the image, occurring approximately 20-30 km offshore. In contrast,

the 1992 image (see Figure 6.2) had the highest reflectance values occurring directly along the coast and extending outward from a distance of between 5 to 20 km depending on the location.

To calculate the difference image for the 1992 and 1985 images and the other images (i.e., 1999-1985, 2002-1999, 2002-1985), the Raster Calculator was used. For example, to calculate the difference image between 1992 and 1985, the expression used in the Raster Calculator window was: Sed_9285_Diff = Seds_1992 - Seds_1985. On the left side of the expression is the name of the output image (Sed_9285_Diff), and on the right side is the specified minus operation which subtracts the 1985 raster from the 1992 raster. The output image for the 1992 to 1985 period is shown in Figure 6.5. It is evident from the output image that a legend category is used in each of the output images to indicate positive or negative changes in sediment concentrations.

6.4.2 Interpretation of Legend Categories in Difference Output Images

In Figure 6.5, the legend categories ranged from -2 to 2. The legend category of 0 indicates areas of relatively no change between those areas in the original images for 1985 (Figure 6.1) and 1992 (Figure 6.2). The legend categories less than 0 indicate areas of reduction in sediments since 1985 whereas the legend categories greater than 0 in Figure 6.5 indicate areas of gain in sediments since 1985.

It could be seen in Figure 6.5 that areas directly offshore (legend categories 1 and 2) showed increases in DN Ranges, thereby reflecting gains in sediment due to increased

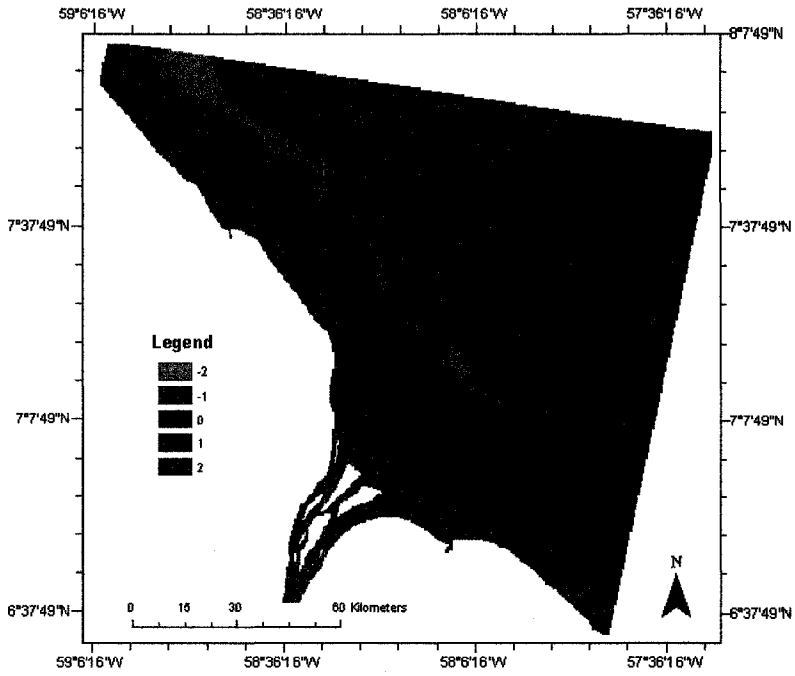

Figure 6.5: Difference Image for 1992 Minus 1985

reflectance in 1992. It could be noted that the maximum DN Range loss is legend category -2, the narrow region approximately 20 to 45 km offshore.

6.5 Percentage Change Differentiation of Images

To obtain insights on the percentage change of sediments in the two time periods, the output attribute table was examined. It could be seen from Figure 6.6 and its associated attribute table (Table 6.1) that most of the cells in the difference image fell into legend category -1. This region is well offshore in most of the image except for the extreme northwest area where it is either directly offshore or within 2 km of the coast.

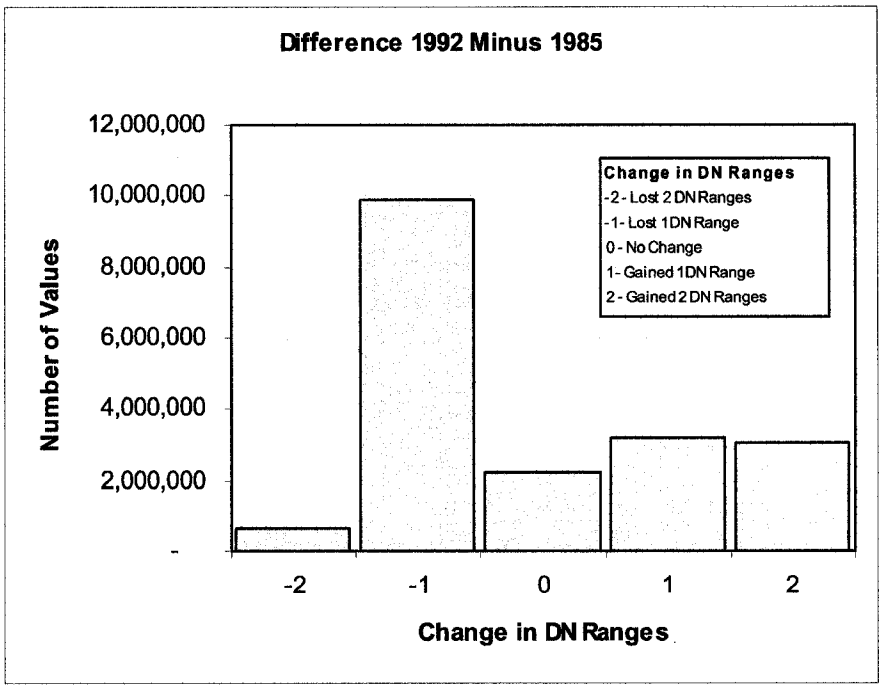

Figure 6.6: Bar Chart for Difference Image: 1992 Minus 1985

Table 6.1: Attribute Table for 1992 Minus 1985

Change	Count	Percentage
-2	667,887	3.49%
-1	9,921,612	51.91%
0	2,264,884	11.85%
1	3,210,937	16.80%
2	3,047,424	15.94%
Total	19,112,744	100.00%

Legend category 0 is indicative of no change in DN Range and accounted for only 11% of the image. It could be seen from Figure 6.5 that sediment concentration, represented by legend categories 1 and 2, increased in the coastal area from 1985 to 1992.

This area comprised 32.74% of the image (see Table 6.1). The nearshore area showed sediment increased since 1985. Hence, between 1985 and 1992, 32.74% of the difference image showed gains in DN Ranges (see Figures 6.5 and 6.6, and Table 6.1),

thereby establishing the fact that suspended sediments increased in the coastal environment between the 1985 to 1992 period. In addition to the difference map and attribute table the output results also included a percentage difference map. Figure 6.7 is an example of the percentage difference map highlighting the spatial areas where sediment changes have occurred.

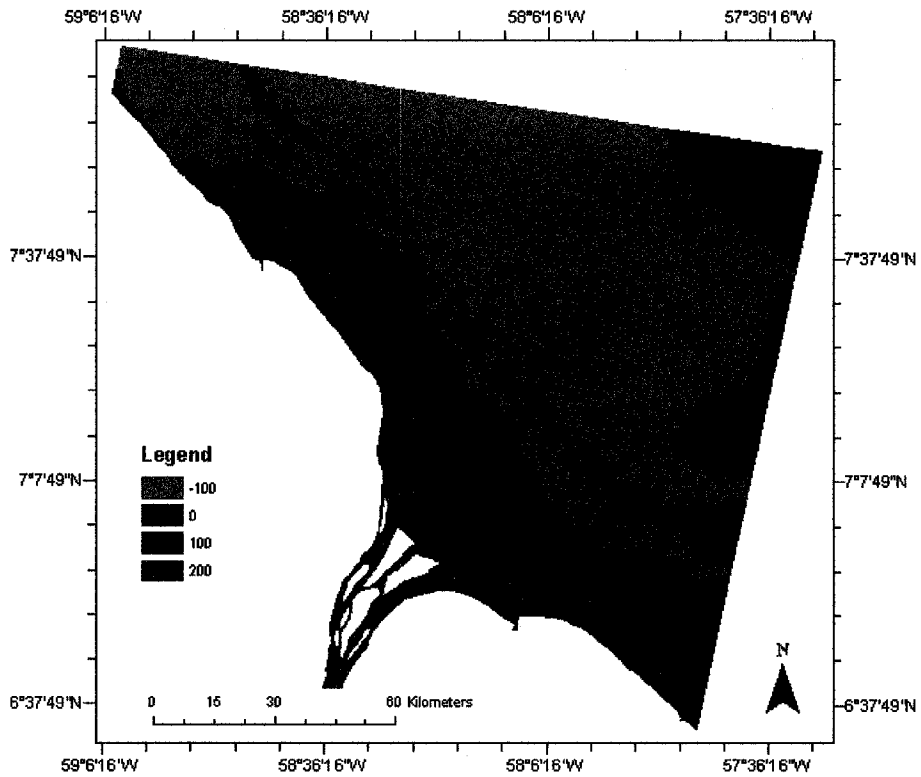

Figure 6.7: Percentage Change Difference Map for the 1992 Minus 1985 Period

6.6 Difference and Percentage Difference Results for the 1999-1985, 1999-2002 and 2002-1985 Periods

6.6.1 Difference Between 1999 and 1985

It could be seen from Figures 6.1 and 6.3 that the 1985 image had lower reflectance values than the 1999 image because the 1985 image had legend categories of 1 to 3, whereas the 1999 image had legend categories 2 to 5 representing DN Ranges of approximately 20 to 100. In Figure 6.3, the brightest reflectance values occurred directly along the coastal area indicated by legend categories 4 and 5. At the mouth of the Essequibo River this area extended approximately 30 km offshore.

When the two images were differenced it was found that 4 legend categories were greater than 0 indicating gains in DN Range. Legend categories 3 and 4 occurred in areas directly offshore along most of the coastal area except for a region in the extreme northwest which showed DN Range of loss or no change.

From the difference image (Figure 6.8) the largest increase in sediment was represented by legend category 4, a gain of 4 DN Ranges. An examination of the attribute table (Table 6.2) indicated that the 1999 image gained 44.69% (i.e., percentage total of legend categories 1-4) more sediments than the 1985 image.

6.6.2 Difference Between 1999 and 2002

Figure 6.3 had a distinct region of DN Range 20-40 in the far offshore area of the image for 1999 with a narrow band of DN Range 40-60 in the middle of the image. In

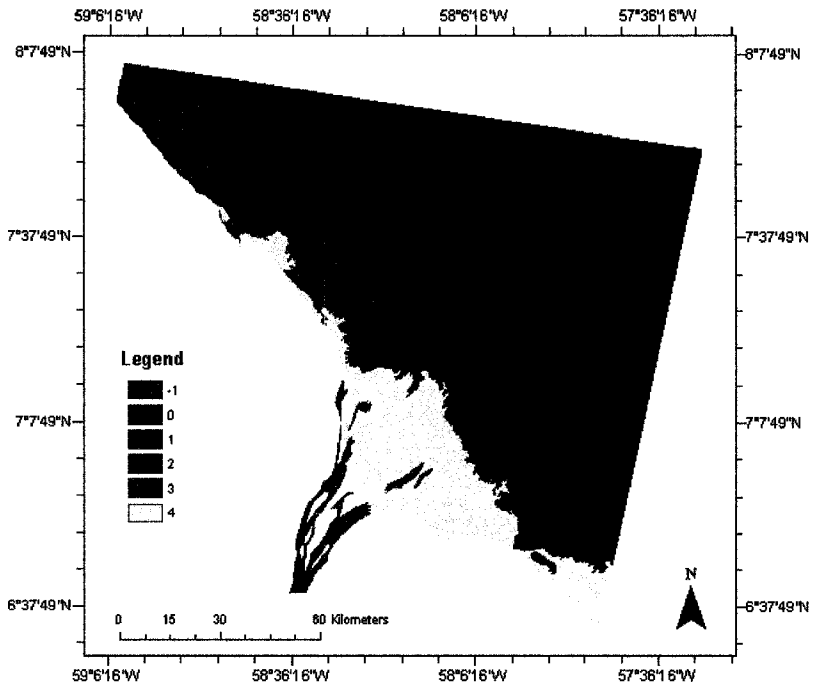

Figure 6.8: Difference Image for 1999 Minus 1985

Table 6.2: Attribute Table for 1999 Minus 1985

Change	Count	Percentage
-1	1,717,510	8.98%
0	8,856,533	46.33%
1	2,820,987	14.76%
2	1,360,724	7.12%
3	1,854,305	9.70%
4	2,507,074	13.11%
Total	19,117,133	100.00%

Figure 6.4, there were no distinct corresponding DN Ranges spanning the entire image. DN Range 20-40 was primarily in the northwest corner, DN Range 40-60 was in the middle and northwest nearshore area while DN Range 80-100 covered the eastern area of the image.

After differencing the image with the Raster Calculator it could be observed from Figure 6.9 there was a definite increase in sediment concentration for the 1999 to 2002 period. This increase was represented by legend category 1 representing a gain of 26.13% and legend category 3 representing a gain of 29.94%. Legend category 3 was almost exclusively located in the eastern edge of the image. Legend category 2 which represented a gain of two DN ranges was only 5.11% of the image, and was located in the eastern section of the image where some areas came to within 1 km of shore, and near the islands of the Essequibo River. From the attribute table (Table 6.3) sediments increased by 61.18% in this time period.

6.6.3 Difference Between 2002 and 1985

From Figures 6.1 and 6.4 it is evident that the 1985 image had lower reflectance values than the 2002 image. The 2002 image had DN Ranges ranging from 20 to 60 and 80 to 130. No values for 60 to 80 were classified for the 2002 image. In Figure 6.4, it could be seen that the brightest reflectance values occurred directly along the coastal area indicated by legend categories 5 and 6. A narrow band extended along the nearshore in the northwest area of the image whereas broader areas were found at the mouth of the Essequibo River, and in the southeastern area of the image. The large area of DN Range 5 in the middle-eastern section of the image represented the clouded area in the original Landsat image.

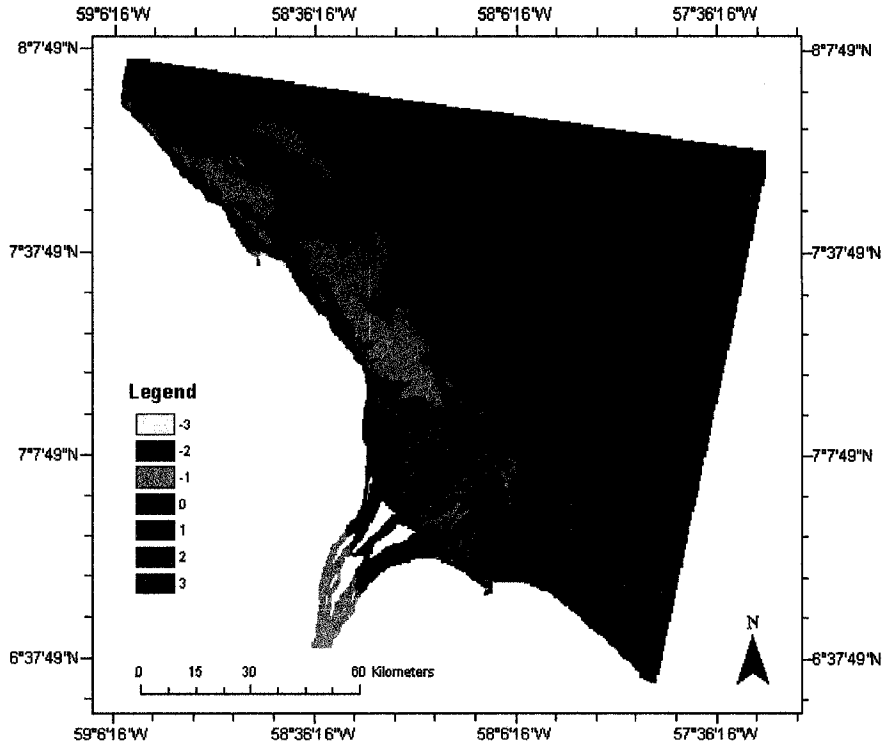

Figure 6.9: Difference Image for 2002 Minus 1999

Table 6.3: Attribute Table for 2002 Minus 1999

Change	Count	Percentage
-3	10,392	0.05%
-2	675,180	3.53%
-1	1,411,962	7.39%
0	5,322,354	27.84%
1	4,996,227	26.13%
2	976,493	5.11%
3	5,724,497	29.94%
Total	19,117,105	100.00%

When the two images were differenced (Figure 6.10) 5 legend categories were greater than 0, and therefore were associated with increases in sediment concentrations. The largest area of increases in sediment concentration was legend category 4 which included areas along the nearshore, and the deeper offshore areas in the eastern edge of

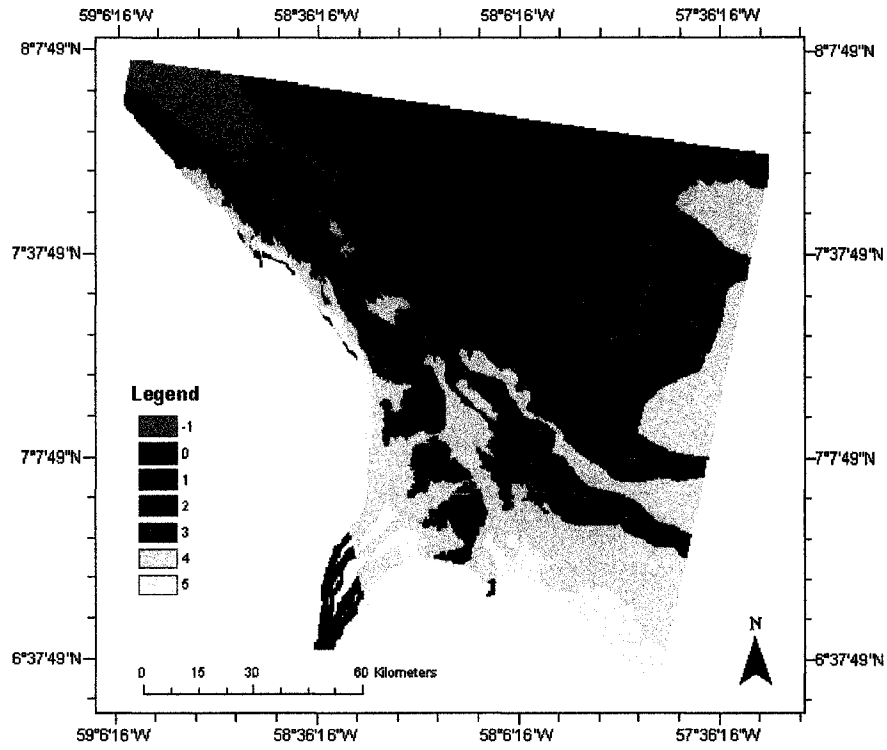

Figure 6.10: Difference Image for 2002 Minus 1985

the image. There was also a noticeable gain in DN Range in legend category 5 which accounted for only 3.4% of the image values. Legend categories 1, 2 and 3 accounted for approximately 52% of the image, with legend category 2 occupying large areas in the nearshore region. Legend category 1 appeared mostly in the center of the image with a smaller region noticeable in the islands of the Essequibo River, whereas legend category 3 was mainly in the deeper water areas in the eastern portion of the image

For the period 1985-2002, approximately 78.6% of the image represented gains in DN Range (see Table 6.4). In the northwest corner of the study area a noticeable loss (4.22%) of sediments occurred. The only portion of the study area which did not show

any gains or losses in sediments was in the northwest corner which was in deeper water, approximately 30 km offshore.

Table 6.4: Attribute Table for 2002 Minus 1985

Change	Count	Percentage
-1	806,548	4.22%
0	3,272,205	17.12%
1	2,706,936	14.16%
2	3,817,301	19.97%
3	3,496,179	18.29%
4	4,368,029	22.85%
5	649,981	3.40%
Total	19,117,179	100.00%

CHAPTER 7

7.0 DISCUSSION AND CONCLUSION

7.1 Discussion

The research for this thesis involved the utilization of several image processing procedures and GIS techniques in order to facilitate fulfilling the objectives and testing of the stated hypotheses of the study. The application of various remote sensing and GIS methodological principles and techniques facilitated the acquisition of results to examine both hypotheses.

The first hypothesis was accepted because appropriate bands were statistically extracted to demonstrate that suspended sediments are associated with specific bands of the electromagnetic spectrum. The PCA was successful in discriminating and isolating a specific band from the MSS, TM and ETM+ sensors. Of the four MSS bands analyzed by the PCA it was found that Band 2, with a wavelength range of 0.6 - 0.7 micrometers, was the best indicator of suspended sediments. The seven wavelength bands of the TM sensor for the 1992 image was reduced to Band 3 (0.63 - 0.69 micrometers) as being the most pronounced in recognizing suspended sediments. For the 1999 image, Band 2 (0.52 - 0.60 micrometers) from the seven ETM+ bands was the most sensitive in discriminating suspended sediments. Of the seven ETM+ bands for the 2002 image, Band 3 (0.63 - 0.69 micrometers) was highly effective in recording the presence of suspended sediments.

Of the twenty-five spectral bands which were examined, this thesis was successful in highlighting the fact that only two spectral bands (Bands 2 and 3) were associated with suspended sediments in coastal waters. Hence, a strong relationship exists between

suspended sediment concentrations and spectral radiance in the wavelength range stretching from 0.52 - 0.70 micrometers. This finding is in agreement with those advanced by other investigators who examined the relationship between suspended sediments and spectral wavelengths. The early study by Jacobberger et al. (1983) found that the wavelength range of between 0.5 and 0.8 micrometers was the best for detecting suspended sediments. More recent studies by Dekker et al. (2002) and Chen et al. (2004) found that suspended sediments are highlighted in 0.52 - 0.69 micrometer spectral range. The close agreement of the results of this thesis with those of other investigators will provide remote sensing investigators with the necessary spectral information for use in remote sensing investigations on suspended sediments in coastal waters.

The remote sensing and GIS based findings also substantiate the observations of field investigators (Allersma, 1971; Eisma and van der Marel, 1971) who found that the Guyana coast is dominated by sediments. An examination of the difference maps and associated attribute tables for the four time periods highlight the fact that sediments have increased in each of the four time periods. A regression plot (Figure 7.1) of the sediment percentage gain data in the attribute tables clearly illustrate the linear increase in suspended sediments for the period 1985 to 2002. This noticeable increase of sediments allows acceptance of the hypothesis that there is a distinct temporal increase of suspended sediment in the nearshore areas of the coastal environment of Guyana. The overall pattern of increase in the coastal environment could be demonstrated with the percentage gain map (Figure 7.2) for the period 1985 to 2002. From the percentage gain map the most pronounced sediment gains are associated with the Guiana Current. The main flow

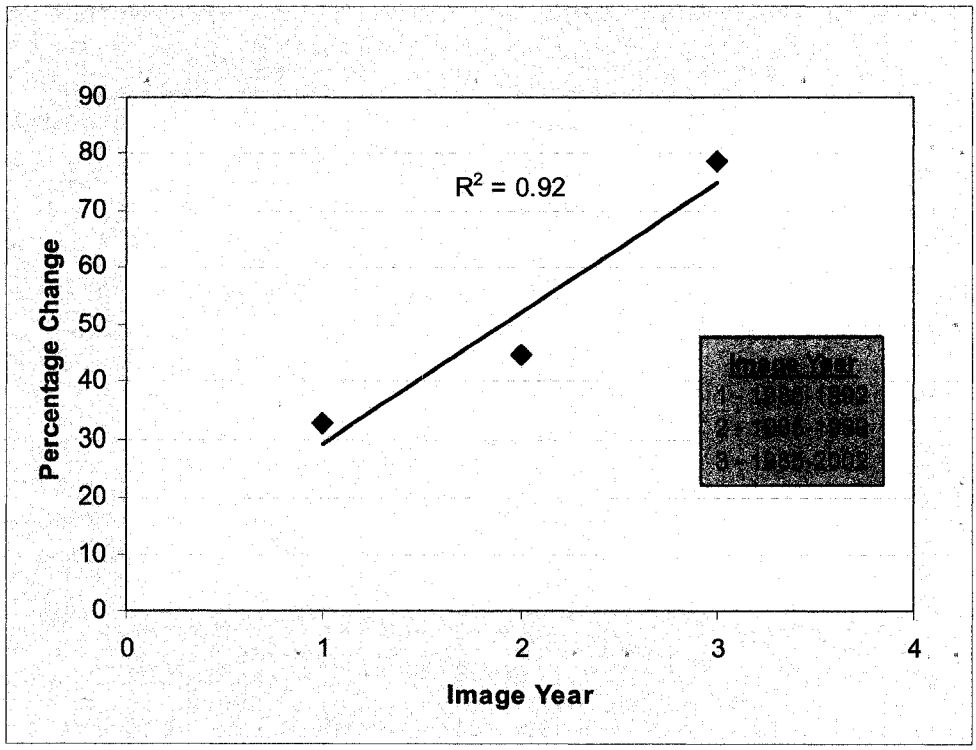

Figure 7.1: Regression Plot of Gains in Suspended Sediments for the Period 1985-2002

component of the Guiana Current, running parallel to the coast, is characterized by a 5 to 10 km band of intense sediment movement. Flanking both sides of the main current channel are two broad bands of sediments moving in a northwesterly direction. Interestingly, the bands of sediments moved by the Guiana Current have become considerably wider over time thereby providing visual evidences of increases in the amount of sediments in the coastal zone. *In situ* measurements have found that sediments increased from 432 mg/l from 1984 to 772 mg/l in 2005 in the location near to Georgetown.

In addition to the influence of currents it is also apparent that the Essequibo River is adding a comparatively small, but significant, amount of sediments to the nearshore

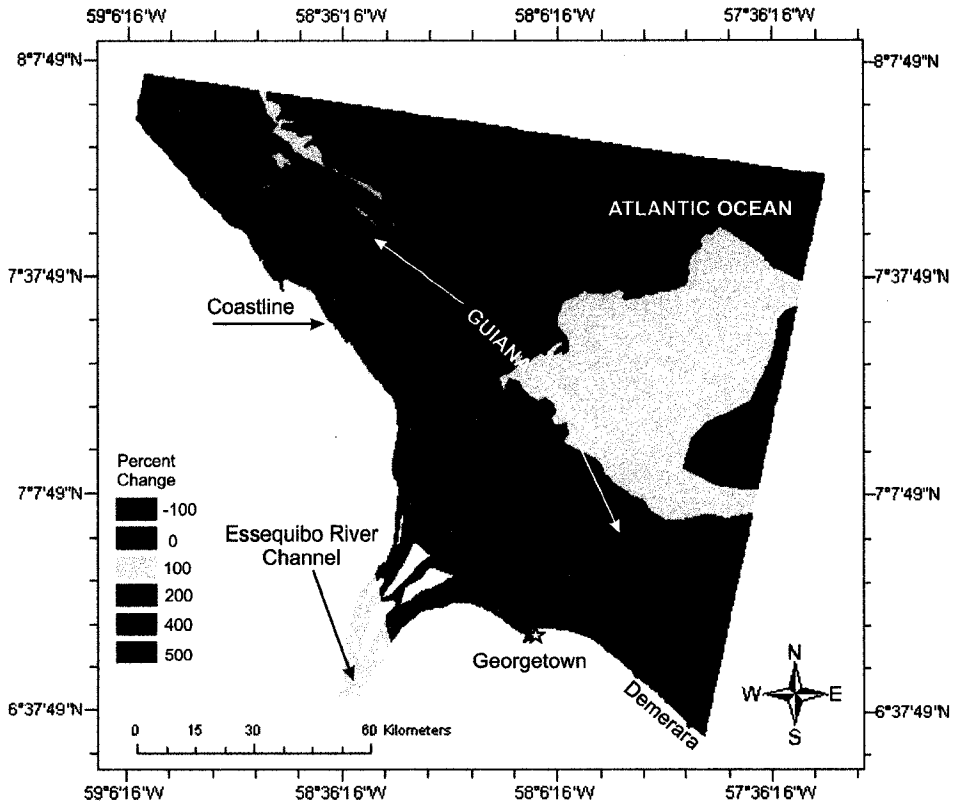

Figure 7.2: Percentage Difference Image Emphasizing Changes in Suspended Sediment Patterns for the Period 1985-2002 (Zero indicates no change; 100 and above refer to increasing percentage changes).

zone. Temporal increases in sediments from the Essequibo River could be observed. It could be inferred that the Essequibo River has, over time, increased its sedimentary load because of erosion from intensive contemporary logging operations in several areas within its watershed. Evidently, one of the consequences of logging in Guyana and ongoing deforestation in the Amazon Basin is the increase in suspended sediments in the coastal waters off the Guyana coast.

7.2 Conclusion

The results of this research lend support to the statement that "the integration of remotely-sensed data, GPS, and GIS technologies provides a valuable tool for monitoring and assessment of waterways". The evolution of satellite technologies has the potential of providing repetitive and high resolution data for the assessment of suspended sediments in coastal and other water bodies. As demonstrated in this study, with rigorous statistical processing of image data valid conclusions could be drawn on the appropriateness of certain spectral bands for discriminating suspended sediments. When analyzed in a GIS, it is possible to map not only the spatial distributions of sediments, but also to monitor temporal variations in sediment concentrations. In the case of the Guyana coast, the loadings of suspended sediments in the coastal zone has increased with time, and the GIS has successfully demonstrated that there are greater and wider dispersal of sediments in the near and offshore waters. Satellite-based remote sensing due to its repetitive multispectral and synoptic nature provides a major advantage over *in situ* measurements for investigating and monitoring where concentrations of suspended sediments could have detrimental impacts on coastal water quality and marine ecosystems.

7.3 Recommendation for Future Work

The increases in sediments in coastal and estuarine areas is now a world-wide problem (Clarke, 1999). requires immediate attention because "increasing rates of sediment loading adversely affect the biodiversity and ecological value of estuarine and coastal ecosystems" (Thrush et al., 2004, p. 299). It is, therefore, strongly recommended

that coastal resource managers and policy planners in Guyana and elsewhere employ remote sensing and GIS techniques to monitor and assess the loadings of suspended sediments in the coastal zone. Remote sensing and GIS results must be supplemented on a regular basis by *in situ* measurements. A country like Guyana must, therefore, implement a scientific program for the acquisition and processing of sedimentological data collected from coastal waters. By calibrating and integrating multi-temporal remote sensing data sets coastal resource managers can employ a GIS-based methodology for not only mapping the temporal and spatial distribution of suspended sediments, but also for forecasting long term trends in coastal water quality.

REFERENCES

1. Allersma, E., 1971. Mud on the Oceanic Shelf Off Guiana. Symposium on Investigations and Resources of the Caribbean Sea and Adjacent Regions. UNESCO, France: Imprimerie Louis-Jean, pp. 193-203.
2. Augustinus, P.G.E.F., 1987. The Geomorphologic Development of the Coast of Guyana Between the Corentyne River and the Essequibo River. In: Gardiner, V. (ed.), International Geomorphology, 1986. Part 1. Utrecht, The Netherlands: Wiley, pp. 1281-1293.
3. Baghdadi, N., Gratiot, N., Lefebvre, J.P., Oliveros, C. and Bourguignon, A., 2004. Coastline and Mud Bank Monitoring in French Guiana: Contributions of Radar and Optical Satellite Imagery. Canadian Journal of Remote Sensing, 30: 109-122.
4. Bhargava, D.S., and Mariam, D.W., 1990. Spectral Reflectance Relationships to Turbidity Generated by Different Clay Material. Photogrammetric Engineering and Remote Sensing, 56: 225-229.
5. Chen, X., Li, Y.S., Liu, Z., Yin, K. and Li, Z., 2004. Integration of Multi-source Data for Water Quality Classification in the Pearl River Estuary and its Adjacent Coastal Waters of Hong Kong. Continental Shelf Research, 24: 1827-1843.
6. Clark Labs, 2004. Idrisi Kilimanjaro version 14.002. Clark University, Worcester, MA.
7. Clarke, R. (Editor), 1999. GEO 2000. Global Environment Outlook. Earthscan Publications.

8. Curran, P.J., Hansom, J.D. and Plummer, S.E., 1987. Multispectral Remote Sensing of Nearshore Suspended Sediments: A Pilot Study. International Journal of Remote Sensing, 8 (l): 103-112.

9. Curran, P.J. and Novo, E.M.M., 1988. The Relationship Between Suspended Sediment Concentration and Remotely Sensed Spectral Radiance: A Review. Journal of Coastal Research, 4: 351-368.

10. Dekker, A., Vos, R. and Peters, S., 2002. Analytical Algorithms for Lake Water Tsm Estimation for Retrospective Analyses of TM and SPOT Sensor Data. International Journal of Remote Sensing, 23: 15-35.

11. Delft Hydraulics Laboratory, (1962. Demerara Coastal Investigation. Report on Siltation of Demerara Bar Channel and Coastal Erosion in British Guiana. Delft, The Netherlands.

12. Doxaran, D., Froidefond, J.M. and Castaing, P., 2002a. A Reflectance Band Ratio Used to Estimate Suspended Matter Concentrations in Sediment-dominated Coastal Waters. International Journal of Remote Sensing, 23: 5079-5085.

13. Doxaran, D., Froidefond, J.M., Lavender, S. and Castaing, P., 2002b. Spectral Signature of Highly Turbid Waters - Application with Spot Data to Quantify Suspended Particulate Matter Concentrations. Remote Sensing of Environment, 81: 149-161.

14. Doxaran, D., Froidefond, J.M. and Castaing, P., 2003. Remote-sensing reflectance of turbid sediment-dominated waters. Reduction of sediment type variations and

changing illumination conditions effects by use of reflectance ratios. Applied Optics, 42: 2623-2634.

15. Doxaran, D., Cherukuru, N.C., Lavender, S.J. and Moore, G.F., 2004a. Use of a Spectralon Panel to Measure the Downwelling Irradiance Signal: Case Studies and Recommendations. Applied Optics, 43: 5981-5986.

16. Doxaran, D., Cherukuru, R.C.N. and Lavender, S.J., 2004b. Estimation of Surface Reflection Effects on Upwelling Radiance Field Measurements in Turbid Waters. Journal of Optics a-Pure and Applied Optics, 6: 690-697.

17. Eisma, D. and van der Marel, H.W., 1971. Marine Muds Along the Guyana Coast and Their Origins from the Amazon Basin. Journal of Mineralogy and Petrology 31: 321-334.

18. ESRI, 2006. ESRI World Base Map Data. The data were available via www.esri.com/data/download/basemap/index.html. Environmental Systems Resource Institute, Redlands, CA.

19. Estournel, C., Kondrachoff, V., Marsaleix, P. and Vehil, R., 1997. The plume of the Rhone: numerical simulation and remote sensing. Continental Shelf Research, 17: 899-924.

20. Forget, P. and Ouillon, S., 1998. Surface Suspended Matter Off the Rhone River Mouth from Visible Satellite Imagery. Oceanologica Acta, 21 (6): 739-749.

21. Froidefond, J.M., Lahet, F., Hu, C., Doxaran, D. and Guiral, D., 2004. Mudflats and Mud Suspension Observed from Satellite Data in French Guiana. Marine Geology, 208: 153-168.

22. Fromard, F., Vega, C. and Proisy, C., 2004. Half a Century of Dynamic Coastal Change Affecting Mangrove Shorelines of French Guiana. A Case Study Based on Remote Sensing Data Analyses and Field Surveys. International Journal of Marine Geology ,Geochemistry and Geophysics, 208: 265-280.

23. González, E., 2005. Dynamics of River Plumes as Detected by AVIRIS. Undergraduate Research Thesis, Geology Department, University of Puerto Rico, Mayaguez.

24. Islam, M.R., Yasushi, Y. and Katsuro, O., 2001. Suspended sediment in the Ganges and Brahmaputra Rivers in Bangladesh: observation from TM and AVHRR Data. Hydrol. Process, 15: 493-509.

25. Jacobberger, P.A., Arvidson, R.E. and Rashka, D.L., 1983. Application of LANDSAT Multispectral Scanner Data and Sediment Spectral Reflectance Measurements to Mapping of the Meatiq Dome, Egypt. Geology, 11: 587-591.

26. Jensen, J.R., 1986. Introductory Digital Image Processing. Prentice-Hall, New Jersey.

27. Johnson, R. and Harris, R., 1980. Remote Sensing for Water Quality and Biological Measurements in Coastal Waters. Photogrammetric Engineering and Remote Sensing, 46: 77-85.

28. Jolliffe, I.T., 2002. Principal Components Analysis. Second Edition. Springer, Berlin, 502p.

29. Khorram, S. and Cheshire, M.H., 1985. Remote sensing of water quality in the Neuse river estuary, North Carolina. Photogrammetric Engineering and Remote Sensing, 53: 329-341.

30. Kiyomoto, Y., Kazuo, I. and Kazumaro, O., 2001. Ocean Color Satellite Imagery and Shipboard Measurements of Chlorophyll a and Suspended particulate Matter Distribution in the East China Sea. Journal of Oceanography, 57: 37-45.

31. Klemas, V., Borchardt, J.R. and Treasure, W.H.., 1973. Suspended Sediment Observations from ERTS-1. Remote Sensing of Environment, 2 (4): 205-221.

32. Lakhan, V.C., 1991. Simulating the Interactions of Changing Nearshore Water Levels, Morphology and Vegetation Growth on Guyana's Coastal Environment. In: McLeod, J. (ed.), Toward Understanding Our Environment. Simulation Councils, Inc., San Diego, CA, pp. 13-20.

33. Lakhan, V.C., 1993. Image Processing Techniques to Evaluate Actual and Potential Degradation of Guyana's Coastal Wetlands. Commonwealth Geographical Bureau Congress, August 13-29, 1993, University of Guyana, Georgetown, Guyana. Manuscript, 47p.

34. Lakhan, V.C., 1994. Planning and Development Experiences in the Coastal Zone of Guyana. Ocean and Coastal Management, 22: 169-186.

35. Lakhan, V.C. and Pepper, D.A., 1997. Relationship Between Grain Size and Heavy Metals in Sediments from Beaches Along the Coast of Guyana. Journal of Coastal Research, 19 (3): 600-608.

36. Lakhan, V.C. and Ahmad, S.R. 2005. Application of Remote Sensing to Assess Suspended Sediments Along Guyana's Coast. Canadian Association of Geographers. Abstract.

37. Lakhan, V.C., Cabana, K. and LaValle, P.D., 2002. Heavy Metal Concentrations in Surficial Sediments from Accreting and Eroding Areas Along the Coast of Guyana. Environmental Geology, 42: 73-80.

38. Lakhan, V.C., Kanyaya, J. and Karki, R., 2004. Assessing and Predicting Coastline Positional Changes. Canadian Association of Geographers, Ontario Division. Program and Abstracts, October 29-30, 2004.

39. Lathrop, R., 1992. Landsat Thematic Mapper Monitoring of Turbid Inland Water Quality. American Society of Photogrammetry and Remote Sensing, 58: 465-470.

40. Li, R-R., Yorman, J.K., Gao, B-C. and Davis, C.O., 2003. Remote Sensing of Suspended Sediments and Shallow Coastal Waters. IEEE Transaction on Geoscience and Remote Sensing, 41: 559.

41. Lillesand, T.M., and Kiefer, R.W., 1994. Remote Sensing and Image Interpretation. John Wiley and Sons, New York.

42. MacKinnon, D.J., Chavez Jr, P.S., Fraser, R.S., Niemeyer, T.C. and Gillette, D.A., 1996. Calibration of Goes-vissr, Visible-band Satellite Data and its Application to the Analysis of a Dust Storm at Owens Lake, California. Geomorphology, 17: 229-248.

43. Maktav, D., Erbek, F.S. and Kabdasli, S., 2002. Monitoring Coastal Erosion at Black Sea Coasts in Turkey Using Satellite Data: a Case Study at the Lake Terkos, North-west Istanbul. International Journal of Remote Sensing, 23: 4115-4124.

44. Mancebo, F.F., Bruce, R.C., Catalan, Z.B., Lim suan, M.P. and Malayang III, B.S., 1997. Correlation of Total suspended Sediments and Reflectance of Landsat TM in Laguna De Bay, Philippines, http://www.gisdevelopment.net/aars/acrs/1997/ts2/ts2003a.shtml

45. Merry, C.J., Zhang, L., and Lin, S.-S., 2006. Using Landsat 7 and MODIS Data for Measuring Suspended Sediment in Lake Erie, North-central Section, GSA. 40th Annual Meeting. Geological Society of America Abstracts with Programs. University of Akron, Akron, OH.

46. Mikkelsen, O.A., 2002. Variation in the projected surface area of suspended particles: implications for remote sensing assessment of TSM. Remote Sensing of Environment, 79: 23-29.

47. Mobasheri, M.R., 2005. Effects of Suspended Sediment Composition on Remotely Sensed SSC in Surface Waters Using MODIS Images. In: Erasmi, B.C.S., and Kappas, M. (Editors), First Gottingen GIS and Remote Sensing Days; Environmental Studies, Gottingen. Remote Sensing and GIS for Environmental Studies, Applications in Geography, Goettinger Geographische Abhandlungen. Geitze, Gottingen, Federal Republic of Germany, pp. 167-174.

48. Mobasheri,M.R. and Hamid, M., 2004. Remote Sensing of Suspended Sediments in Surface Waters, Using MODIS images. http://www.isprs.org/istanbul2004/comm7/papers/244.pdf

49. Nellis, M.D., Harrington, J.J.A. and Wu, J., 1998. Remote Sensing of Temporal and Spatial Variations in Pool Size, Suspended Sediment, Turbidity, and Secchi depth in Tuttle Creek Reservoir, Kansas:1993. Geomorphology, 21: 281-293.

50. Olariu, C., Stern, R.J., and Bhattacharya, J.P., 2002. The Red River Delta, Lake Texoma: A Remote Sensing Study of Delta, South-central Section. 36th Annual Meeting, Department of Geosciences, University of Texas at Dallas.

51. Ouillon, S., Douillet, P. and Andrefouet, S., 2004. Coupling Satellite Data with in Situ Measurements and Numerical Modeling to Study Fine Suspended-sediment Transport: a Study for the Lagoon of New Caledonia. Coral Reefs, 23: 109-122.

52. Puls, W., Doerffer, R. and Sundermann, J., 1994. Numerical simulation and satellite observations of suspended matter in the North Sea. IEEE Journal of Ocean Engineering, 19: 3-9.

53. Ritchie, J.C., 2005. Remote sensing techniques for determining suspended sediments. Presented at the Eighth Conference on Remote Sensing for Marine and Coastal Environments, Halifax, Nova Scotia, 17-19 May 2005, 8p.

54. Ritchie, J.C. and Cooper, C.M., 1988. Comparison on Measured Suspended Sediment Concentrations with Suspended Sediment Concentrations Estimated from Landsat Mss Data. International Journal of Remote Sensing, 9: 379-387.

55. Ritchie, J.C., Cooper, C.M. and Schiebe, F.R., 1990. The Relationship of MSS and TM Digital Data with Suspended Sediments, Chlorophyll, and Temperature in Moon Lake, Mississippi. Remote Sensing of Environment, 33: 137-148.

56. Ritchie, J.C., McHenry, J.R., and Schiebe, F.R., 1974. The Relationship of Reflected Solar Radiation and the Concentration of Sediment in the Surface Water of Reservoirs. Remote Sensing of Earth Resources, Vol. III, pp. 57-72.

57. Ritchie, J.C., Schiebe, F.R. and McHenry, J.R., 1976. Remote-Sensing of Suspended Sediments in Surface Waters. Photogrammetric Engineering and Remote Sensing, 42: 1539-1545.

58. Ruddick, K., Ovidio, F., Eynde, D.V.d. and Vasilkov, A., 1998. The Distribution and Dynamics of Suspended Particulate Matter in Belgian Coastal Waters Derived from Avhrr Imagery, 9th Conference on Satellite Meteorology and Oceanography, Paris, pp. 626-629.

59. Siddiqui, M.N. and Maajid, S., 2004. Monitoring of Geomorphological Changes for Planning Reclamation Work in Coastal Area of Karachi, Pakistan. Advances in Space Research, 33: 1200-1205.

60. Tassan, S., 1987. Evaluation of the Potential of the Thematic Mapper for Marine Application. International Journal of Remote Sensing, 8: 1455-1478.

61. Thrush, S.F., Hewitt, J.E., Cummings, V.J., Ellis, J.I., Hatton, C., Lohrer, A., and Norkko, A., 2004. Muddy Waters: Elevating Sediment Input to Coastal and Estuarine Habitats. Frontiers in Ecology and Environment., 2 (6): 299-306.

62. Tolk, B.L., Han, L. and Rundquist, D.C., 2000. The Impact of Bottom Brightness on Spectral Reflectance of Suspended Sediments. International Journal of Remote Sensing, 21: 2259-2268.

63. Topliss, B., Amos, C. and Hill, P., 1990. Algorithms for Remote Sensing of High Concentration, Inorganic Suspended Sediment. International Journal of Remote Sensing, 24: 335-358.

64. Walker, Nan., Roberts, H., Stone, G., Bentley, S. and Huh, O., 2002. Satellite-Based Assessment of Sediment Transport, Distribution and Resuspension Associated with the Atchafalaya River Discharge Plume. Gulf Coast Association of Geological Societies Transactions, 52: 967-973.

65. Welby, C.W.,1978. Application of Landsat Imagery to Shoreline Erosion. Photogrammetric Engineering and Remote Sensing, 44 (9): 1173-1178.

66. Wijekoon, N., Ortiz, J., and Munro_Stasiuk, 2006. Remote Sensing of Total Suspended Particulates in the Western Basin of Lake Erie, North-central Section, GSA. 40th Annual Meeting. Geological Society of America Abstracts with Programs.

67. Xiaoqin, W., Qinmin, W., Gaohuan, L., and Li, H., 2005. A Study on the Quantitative Remote Sensing Model for the Suspended Sediment Concentration in Coastal Waters with ASTER Data. Remote Sensing Symposium, 2005. IGARSS'05. Proceedings. 2005, ieeexplore.IEEE.org

68. You, Y. and Hou, M., 1992. Remote Sensing Analysis of the Suspended Sediment Transport in Lingdingyang. China Ocean Engineering, 6: 331-349.

69. Zhu, X., 2001. Remote Sensing Monitoring of Coastline Changes in Pearl River Estuary, 22nd Asian Conference on Remote Sensing, Singapore.

VITA AUCTORIS

NAME:	Sajid Rashid Ahmad
PLACE OF BIRTH	Pakistan
YEAR OF BIRTH	1967
EDUCATION	University of the Punjab, Lahore, Pakistan 1986-1990 B.Sc.(Three Years Applied Geology) University of the Punjab, Lahore, Pakistan 1991-1993 M.Sc.(Applied Geology) University of Windsor, Windsor, Ontario, Canada 2004-2006 M.Sc.